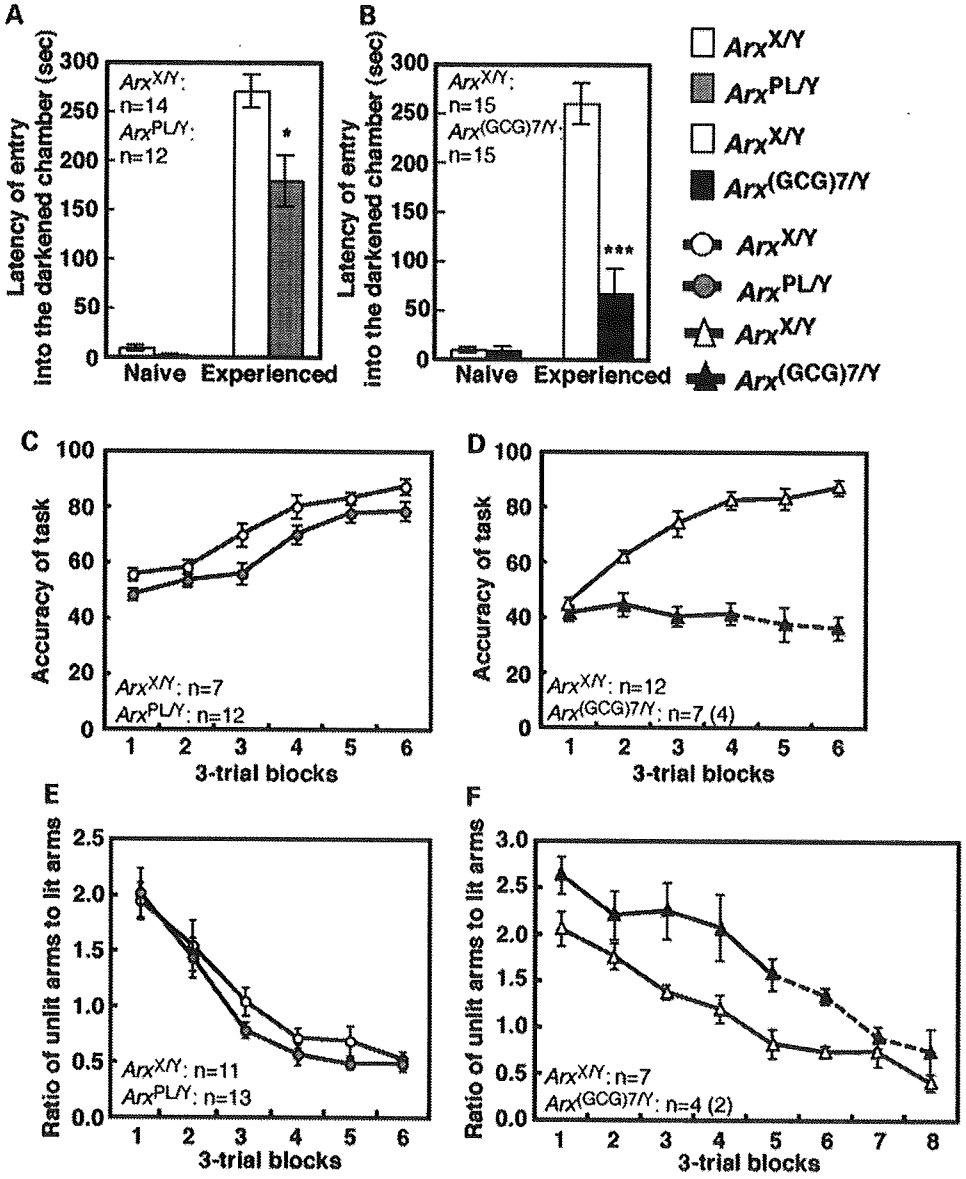

Figure 5. Defects in several aspects of learning and memory in $Arx^{PL/Y}$ and $Arx^{(GCG)7/Y}$ mice. (**A** and **B**) Latency to enter a darkened chamber in the passive avoidance task. The left set of bars represents results before the mice received electric shocks in the darkened chamber; the right set shows the results after shocks. A significant difference from the $Arx^{X/Y}$ mice is represented by * for $P < 0.05$ and *** for $P < 0.001$. (**C** and **D**) Accuracy of the win-shift task on the eight-arm radial maze, which we present as the percentage of chosen arms that were baited. The value is given as the mean of three trials. (**E** and **F**) The ratio of the unlit arm choices to lit arm choices in the win-stay task on the eight-arm radial maze. The value is given in the same manner as (C) and (D). The $Arx^{(GCG)7/Y}$ mice and $Arx^{X/Y}$ mice were statistically analyzed from blocks 1 to 4 in (D) and from block 1 to 5 in (F), using the number of the subjects shown in the figures. Mean values are shown on the solid line. The mean values on the broken line were calculated from the number of surviving $Arx^{(GCG)7/Y}$ mice in each block because some of them died during training. The number of subjects surviving throughout the tasks is shown in the parentheses.

and mental retardation, respectively, without the involvement of any other genetic factors.

The importance of the conserved YPD in the homeodomain was demonstrated in the $Arx^{PR/Y}$ and $Arx^{PL/Y}$ mutant mice (4,7). Proline in the YPD is predicted to have influence on homeodomain structure by providing the proper hydrophobic environment (32), whereas leucine and arginine have stronger and much weaker (hydrophilicity) hydrophobicity compared with proline, respectively (33). Thus, the hydrophobic environment suitable for the normal homeodomain structure and function may be destroyed by each mutation. It was surprising that the (GCG)7 mutation did not result in the specific formation of intranuclear inclusions and apoptosis that were observed in the *in vitro* functional test of the mutation (28,29) and this was also true of the $Arx^{432-455dup/Y}$ mice in our present study (unpublished data). The elongation of the polyalanine tract may function in the downregulation of ARX activity in cooperation with other functional domains of ARX such as homeodomain.

Seizure and ARX-positive neurons

Seizures occurred in most of the $Arx^{(GCG)7/Y}$ mice at P1m, and ~10% died during an episode of status epilepticus, suggesting

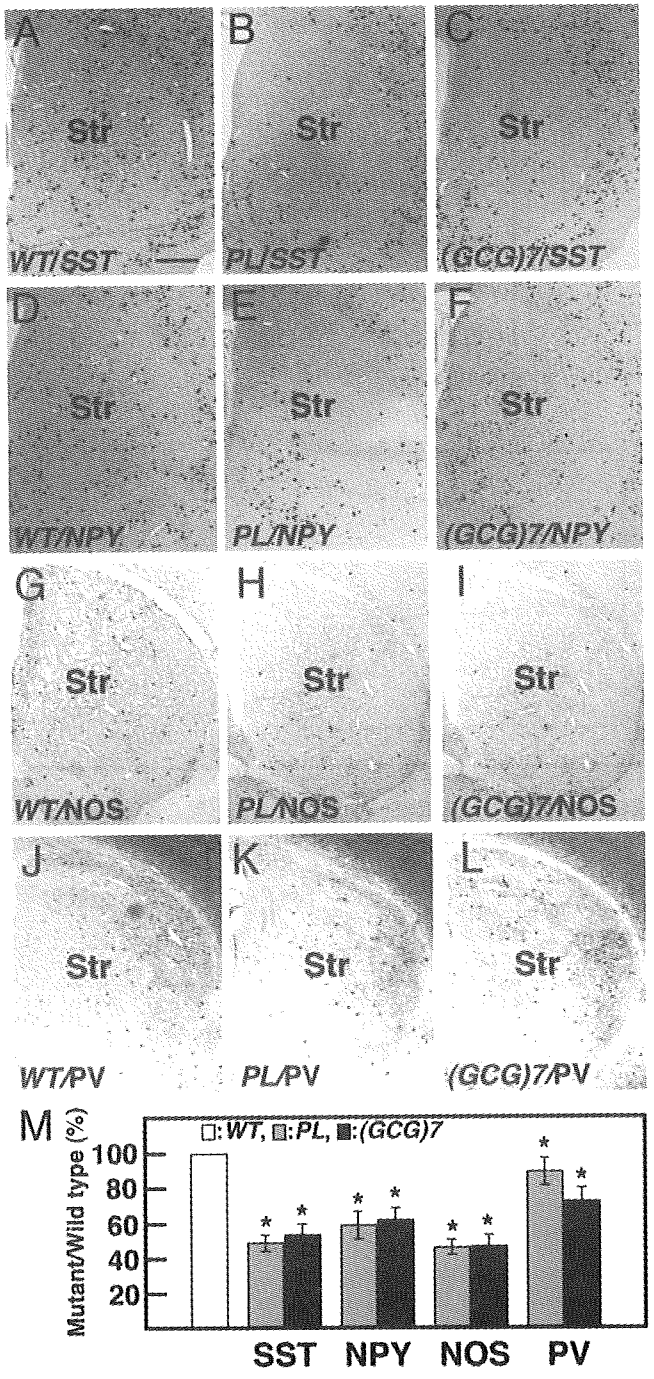

Figure 6. Reduction of neurons in each subtype of GABAergic interneurons in the striatum of $Arx^{PL/Y}$ and $Arx^{(GCG)7/Y}$ mice at P1m. SST^+ interneurons of $Arx^{PL/Y}$ ($47.8 \pm 4.8\%$, $P < 0.001$, $n = 3$. **B, M**) and $Arx^{(GCG)7/Y}$ mice ($52.4 \pm 6.2\%$, $P < 0.001$, $n = 3$. **C,** M) were about half as many cells within the SST^+ interneurons as in $Arx^{X/Y}$ mice (**A**). The same tendency was seen for the NPY^+ (**D–F,** M) and NOS^+ (**G–I,** M) interneurons. In contrast, the reduction in PV^+ interneurons in $Arx^{PL/Y}$ ($85.2 \pm 4.2\%$, $P < 0.01$, $n = 3$. **K,** M) and $Arx^{(GCG)7/Y}$ ($70.6 \pm 7.3\%$, $P < 0.002$, $n = 3$. **L,** M) mice was small compared with the other subtypes. Values in (M) are normalized to the wild-type. Str: striatum. Scale bar: A–L, 500 μm.

that the seizure caused the death. In contrast, only one $Arx^{PL/Y}$ mouse exhibited seizures, which were mild and occurred at 1 month of age. The observation that the longevity of $Arx^{PL/Y}$ mice was not different from that of $Arx^{X/Y}$ mice clearly shows that the seizure phenotype of the $Arx^{PL/Y}$ mice was milder than that of the $Arx^{(GCG)7/Y}$ mice. The onset latency and characteristics of the seizures in the $Arx^{PL/Y}$ mice following a low dose of bicuculline were significantly different from those of the $Arx^{X/Y}$ mice, suggesting that the $Arx^{PL/Y}$ mice had the epileptic phenotype. We conclude that both mutants show the epileptic phenotype that becomes apparent during late infancy to weaning age, albeit with different levels of severity in the two mutants. Interestingly, both types of mutants showed the epileptic phenotype with a severity of seizures that was similar to that in the corresponding human types. Most patients with the (GCG)7 mutations are diagnosed with infantile syndrome, whereas patients with the PL mutation develop myoclonic epilepsy (4). Epilepsy in patients with the (GCG)7 mutation is more severe than that in patients with the PL mutation.

Recently, it has been shown that specific abnormalities in the development or function of cortical GABAergic interneurons are linked to epilepsy (34,35). $Arx^{-/Y}$ mice exhibit interneuron migration deficiencies (3), and the $Arx^{PR/Y}$ mice in our present study were identical or very similar to $Arx^{-/Y}$ mice in this regard. Although $Arx^{-/Y}$ and $Arx^{PR/Y}$ mice did not exhibit seizures because they died around birth, the insuf-

Figure 7. Reduction of cholinergic interneurons in the striatum and cholinergic and GABAergic projection neurons in the medial septum and ventral forebrain nuclei in $Arx^{PL/Y}$ and $Arx^{(GCG)7/Y}$ mice at P1m. (**A–C**) $ChAT^+$ cholinergic interneurons in the striatum. There were about half as many $ChAT^+$ interneurons in $Arx^{PL/Y}$ mice (B) as in $Arx^{X/Y}$ mice (A), whereas no cholinergic interneurons were found in $Arx^{(GCG)7/Y}$ mice (C). (**D–F**) $ChAT^+$ cholinergic projection neurons in the medial septum (MS) and vertical limbs of the nucleus of the diagonal bands (DBv). The number of neurons in the MS of $Arx^{PL/Y}$ mice was reduced to $53.2 \pm 4.8\%$ of that of $Arx^{X/Y}$ mice ($P < 0.001$, $n = 3$, D, E), whereas it was reduced to $23.4 \pm 4.0\%$ of that of $Arx^{X/Y}$ mice in $Arx^{(GCG)7/Y}$ mice ($P < 0.001$, $n = 3$, F). The number of neurons in the DBv of $Arx^{PL/Y}$ mice was reduced compared with the MS. (**G–I**) $GAD67^+$ projection neurons in the MS and DBv. The number of neurons was severely reduced in the MS and DBv of $Arx^{PL/Y}$ mice (H), and no neurons were found in the MS or DBv of $Arx^{(GCG)7/Y}$ mice (I), except for GAD67 signals in the most anterior medial MS and DBv (inset of I). (**J–L**) $ChAT^+$ cholinergic projection neurons in the magnocelular preotic nucleus. The numbers of cholinergic projection neurons in $Arx^{PL/Y}$ (K, P) and $Arx^{(GCG)7/Y}$ (L, P) mice were $80.1 \pm 8.5\%$ ($P < 0.01$, $n = 3$) and $68.4 \pm 7.5\%$ ($P < 0.001$, $n = 3$), respectively, of that in $Arx^{X/Y}$ mice (J). (**M–S**) Acetylcholinesterase $(AchE)^+$ axonal arbors of cholinergic projection neurons in the hippocampus (M–O, S) and cortex (P–S). The total length of $AchE^+$ fibers per arbitral area in the hippocampus (molecular layer of dentate gyrus) of $Arx^{PL/Y}$ (N) and $Arx^{(GCG)7/Y}$ (O) mice was $50.5 \pm 5.2\%$ ($P < 0.01$, $n = 3$) and $16.4 \pm 6.7\%$ ($P < 0.001$, $n = 3$), respectively, of that in $Arx^{X/Y}$ mice (M). The total length of $AchE^+$ fibers per arbitral area in the somatosensory cortex of $Arx^{PL/Y}$ (Q) and $Arx^{(GCG)7/Y}$ (R) mice was $65.5 \pm 9.8\%$ ($P < 0.01$, $n = 3$) and $15.8 \pm 6.6\%$ ($P < 0.001$, $n = 3$), respectively, of that in $Arx^{X/Y}$ mice (P). Values in (S) are normalized to wild-type. Str: striatum, MS: medial septum, DBv: vertical limbs of the nucleus of the diagonal band, MCPO: magnocellular preoptic nucleus, DG: dentate gyrus, Cx: cortex. Scale bars: A–C, 500 μm; D–I, 500 μm; J–L, 500 μm; M–O, 100 μm; P–R, 200 μm; M–O, 100 μm; P–R, 50 μm.

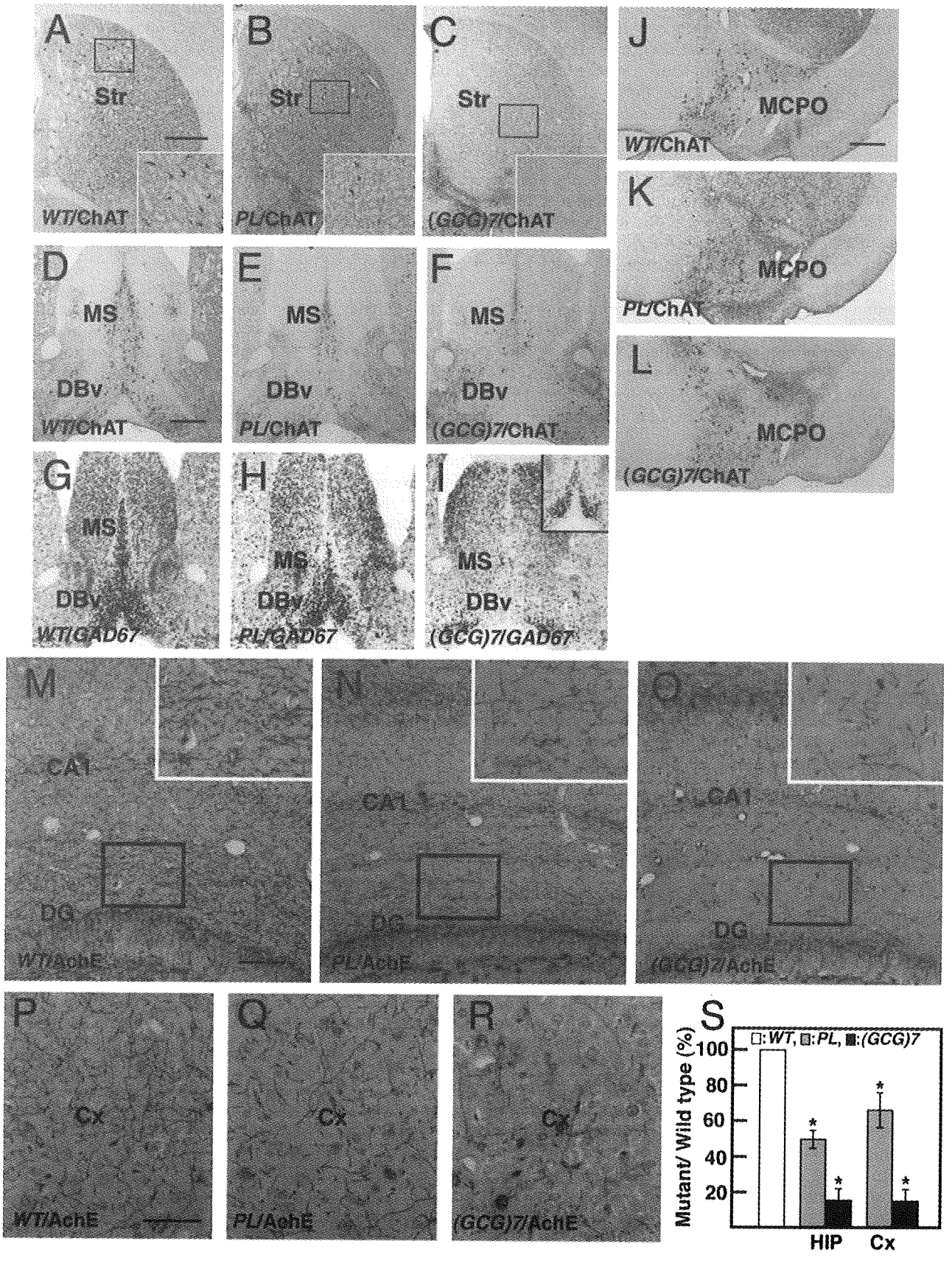
A
Str
WT/ChAT
B
Str
PL/ChAT
C
Str
(GCG)7/ChAT
J
MCPO
WT/ChAT
K
MCPO
PL/ChAT
L
MCPO
(GCG)7/ChAT
D
MS
DBv
WT/ChAT
E
MS
DBv
PL/ChAT
F
MS
DBv
(GCG)7/ChAT
G
MS
DBv
WT/GAD67
H
MS
DBv
PL/GAD67
I
MS
DBv
(GCG)7/GAD67
M
CA1
DG
WT/AchE
N
CA1
DG
PL/AchE
O
CA1
DG
(GCG)7/AchE
P
Cx
WT/AchE
Q
Cx
PL/AchE
R
Cx
(GCG)7/AchE
S
□:WT, ▨:PL, ■:(GCG)7
Mutant/ Wild type (%)
100
80
60
40
20
HIP
Cx

ficient GABAergic interneuron migration may conceivably cause epilepsy in patients with lissencephaly due to the PR mutation. Surprisingly, we found that cortical and hippocampal GABAergic interneurons did not show a marked reduction in the $Arx^{PL/Y}$ or $Arx^{(GCG)7/Y}$ mice, but these mice did have seizures. Previous studies have shown that septal GABAergic projection neurons innervate GABAergic interneurons, and their cholinergic projection neurons form synapses with all neuron types in the hippocampus (36,37). It should also be noted that abolishing septal cholinergic projection neurons facilitated kindling in the hippocampus (38) and that inhibiting $GABA_A$ receptors expressed in GABAergic and cholinergic projection neurons in the septal region induced epileptiform activity in the hippocampus and seizures (39). Our results with the septum raise the possibility that seizures in $Arx^{PL/Y}$ and $Arx^{(GCG)7/Y}$ mice are caused by a loss of cholinergic and GABAergic projection neurons in that region.

We also revealed the loss of the GABAergic interneurons in the striatum. Much experimental evidence has suggested that the basal ganglia play an effective role in controlling seizures in animal epilepsy models (40,41), but the effects of the loss of striatal GABAergic interneurons in epilepsy remain enigmatic. We recorded EEGs in the striatum to examine its involvement in seizure generation and found that spike and burst patterns in the striatum were maintained at high voltage even after the voltage decayed in the hippocampus. Bipolar recording in the striatum also showed high-amplitude waves during the seizures, indicating local generation of epileptic activity. These EEG findings support a significant role of the striatum in seizure generation, although we could not detect the primary locus. The striatum receives input from large cortical areas. Epileptiform activity in the cortex evokes depolarizing bursts that are accompanied by action potentials in striatal projection neurons (42), and neocortical seizure-like EEG oscillations are evoked by tetanization of the striatum (43). Our results suggest that the loss of the GABAergic interneurons that inhibit projection neurons in the striatum may play a role in the epileptic network, inducing status epilepticus.

Impaired learning performance and ARX-positive neurons

Both $Arx^{PL/Y}$ and $Arx^{(GCG)7/Y}$ mice showed defects in several aspects of learning and memory. Passive avoidance is used as an experimental model of amnesia in rodents treated with cholinergic antagonists in the forebrain or striatum (44). Neither mutant could successfully acquire avoidance behavior, and the $Arx^{(GCG)7/Y}$ mice, with their severely impaired cholinergic projection neurons and interneurons, showed a more prominent defect than the $Arx^{PL/Y}$ mice. This observation suggests that these memory defects are due to cholinergic dysfunction in the forebrain of (GCG)7 and PL mutant mice. The win-shift task of the radial maze is a hippocampus-dependent spatial working or episodic-type memory task (45). Both types of mutant mice showed inaccurate performance on this task, with a more severe effect seen in the $Arx^{(GCG)7/Y}$ mice, which did not improve their performance with training. Significant impairment in win-shift performance was produced not by a single lesion in the cholinergic projection neurons in Ch1/2 but by a complex lesion in either the GABAergic projection neurons in Ch1/2 or the cholinergic projection neurons in Ch4 (46). Both types of mutant mice had a coincident reduction or loss of both projection neurons in Ch1/2 and cholinergic projection neurons in Ch4, which likely underlies their inaccurate performance. In the $Arx^{(GCG)7/Y}$ mice, this reduction or loss was more severe than in the $Arx^{PL/Y}$ mice. Moreover, a reduction in the hippocampal PV^+ interneurons could have affected win-shift performance (47) in the $Arx^{(GCG)7/Y}$ mice (data not shown, Supplementary Material, Fig. S6). Thus, these histological differences from the $Arx^{PL/Y}$ mice may have been manifested in the lack of improvement in win-shift performance of the $Arx^{(GCG)7/Y}$ mice. Win-stay performance, which represents striatum-dependent procedural learning (45), was impaired only in the $Arx^{(GCG)7/Y}$ mice in the present study. Cholinergic interneurons, which were reduced in both mutants, play an important role in procedural learning (48,49). The complete loss of the striatal cholinergic interneurons in $Arx^{(GCG)7/Y}$ mice likely led to their inferior win-stay performance. On the other hand, $Arx^{PL/Y}$ mice showed a less severe reduction in striatal cholinergic interneurons and unimpaired win-stay performance.

In conclusion, we reported a causal relationship between three *Arx* mutations and the pleiotropic phenotype using three generated mutant mice. The present mutant mice offer various research opportunities, including elucidation of the molecular properties of *Arx* cascade affected by each mutation and pathogenesis of aberrant neural systems caused by reduction of GABAergic and cholinergic neurons in the forebrain. Thus, these mutant mice could serve as excellent models for research on remarkable pleiotropy of XLAG and mental retardation with epilepsy and, moreover, for reversing the syndromes (50).

MATERIALS AND METHODS

The experiments were conducted in accordance with the animal care regulations of the Mitsubishi Kagaku Institute of Life Sciences, the National Institute of Neuroscience and the Tokyo Institute of Psychiatry.

Construction of the targeting vectors

We constructed three types of targeting vectors in which partial *Arx* fragments (3) containing the different mutations were linearly ligated to the Neo and DTA genes; these DNA fragments were then subcloned into pBluescript II (Fig. 1A and B). The P355R mutation (CCT –> C*g*T) was introduced using the GENEEditor TM *in vitro* Site Directed Mutagenesis System (Promega, WI) and the sense primer 5′-CCAGCGGG AGGAA**CTcGAG**CGGGCTTTCCAGACGCACTACC-***g***TG ACGTCTTCACCCAGG-3′ (the italicized bold lowercase letter shows the mutation site and the newly introduced *Xho*I site is in boldcase) (Fig. 1A). The P355L (CCT –> C*t*T) mutation was introduced by PCR using the sense primer 5′-GGCTGCAGCGGCGGCGGCGGC-3′ and the antisense primer 5′-AAGACGTCA-***a***GGTAGTGCGTCTTCTGGAAA GCCCG**CTCgAG**TTCCTCCAGCTGGTAA-3′ (the italicized bold lowercase letter shows the mutation sit, and the newly introduced *Xho*I site is in boldcase) (Fig. 1A). The addition of seven alanines into the first polyalanine domain was

carried out by inserting 7 × (GCG) into a *Not*I site (325GCGGCCGC332), designated as the '330ins(GCG)7' mutation (GCCGC –> GC*ggcggcggcggcggcggcggc-g*GC); this mutation was introduced by PCR using the sense primer 5′-GGCTGCAGC-GGCGGCG**GCGGC*ggcggcggcggcggcggcggcg*GC**AGCGGCGGCCACGGC-3′ and the antisense primer 5′-AAGACGTCAGGGTAGTGCGT-3′ (the italicized bold lowercase letters show the insertion sequence and the destroyed *Not*I site is in boldcase) (Fig. 1B).

Transfection, screening and generation of three *Arx* mutant mice

To obtain the targeted ES cells, we used a positive–negative selection strategy in the CCE ES cells (a gift from Dr E. Robertson), which are derived from 129/Sv. We screened ES colonies by Southern blot analysis with a 5′ probe and a 3′ probe external to the genomic sequences contained in the targeting vector and a Neo gene (red and blue bars in Fig. 1A and B). Furthermore, we confirmed the introduction of each mutation by Southern blot analysis using the introduced *Xho*I site in the PL and PR mutations or the lost *Not*I site in the (GCG)7 mutation (green bar in Fig. 1A and B). We injected the positive ES clones into (C57BL/6J × BDF1) F1 or C57BL/6J blastocysts, which we then transferred into pseudopregnant female recipients. The resulting chimeric mice were bred with C57BL/6J females. Transmission of the targeted *Arx* locus was confirmed by Southern blot patterns. We obtained three *Arx* mutant mice ($Arx^{mt/Y}$: $Arx^{PR/Y}$, $Arx^{PL/Y}$, $Arx^{(GCG)7/Y}$), which were used in the subsequent analysis by crossbreeding with $Arx^{mt/X}$ and $Arx^{X/Y}$ mice. The $Arx^{mt/Y}$ hemizygotes derived from two independent targeted ES cell lines were phenotypically indistinguishable.

Genome DNA, *Arx* transcript and protein analysis

For Southern blots, we analyzed aliquots of genomic DNA from ES cells or tails of mice by ^{35}P-radioactive filter hybridization (3). For quantitative real-time PCR analysis, we carried out oligo-dT-primed reverse-transcription on aliquots of total RNA from the forebrain at E14.5 and used the single-strand cDNA products. Quantitative real-time PCR was performed with TaqMan primers on an ABI 7300 Real-Time PCR system (Applied Biosystems, CA, USA). All samples were analyzed in triplicate and were normalized relative to glyceraldehyde-3-phosphate dehydrogenase (*Gapdh*) expression, which served as an internal control for each sample. *Gapdh* expression was monitored using TaqMan rodent Gapdh control reagents (Applied Biosystems). We analyzed *Arx* expression using TaqMan Arx primers (Applied Biosystems). Expression levels were normalized to the wild-type for comparison. Data were analyzed with SDS 2.0 (Applied Biosystems) and Microsoft Excel, using the ΔΔCt method and the expression level of *Gapdh* as an internal reference for each sample. We carried out western blot analyses of RIPA buffer-extracted samples using an ARX polyclonal antibody (3). All samples were analyzed in triplicate and were normalized relative to actin expression, and the expression levels were normalized to the wild-type for comparison. Expression was detected by chemiluminescence (ECL, Amersham/GE Healthcare, NJ, USA), and the data were analyzed using the public domain Image J program developed by the US National Institutes of Health.

Histological analysis

Embryos were immersed and fixed in 4% paraformaldehyde (PFA) in phosphate-buffered saline for 12 h, and post-natal animals were fixed by cardiac PFA perfusion. Brains were post-fixed overnight, cryoprotected in a gradient of sucrose to 30%, frozen in embedding medium (OCT, Tissue-Tek) and serially sectioned at a thickness of 10 μm using a cryostat. For immunohistochemical staining, *in situ* hybridization and acetylcholinesterase histochemistry, four to six semi-sequential coronal sections per region (striatum, MS, MCPO, sensory cortex, hippocampus and basolateral amygdala) of three or four wild-type or mutant mice were selected according to the mouse brain atlas (51). Immunohistochemical staining and *in situ* hybridization were carried out as described (3). The antibodies used were anti-ARX antibody (3), anti-PV antibody (Sigma), anti-ChAT antibody (Chemicon/Millipore, MA, USA), anti-NOS antibody (Chemicon), anti-MAP2 antibody (Chemicon), anti-TBR1 antibody (abcam), anti-Foxp1 antibody (abcam) and anti-SATB2 antibody (Bio Matrix Research Inc.). Immunohistochemical signals were visualized by the following systems: (a) peroxidase-labeled secondary antibody/diaminobenzidine, (b) GFP-GAD67 and an anti-ARX antibody intensified with Alexa594-streptavidin (Molecular Probes/Invitrogen, CA, USA) and (c) an antibody intensified with FITC-labeled secondary antibody (Chemicon) and anti-ARX antibody intensified with Alexa594-streptavidin (Molecular Probe). The antisense probes were *Lhx8* (a gift from Dr V. Pachnis), *SST*, *NPY* and *GAD67*. Acetylcholinesterase histochemistry was performed as described previously (52). In each section, the number of positive cells per square micrometer in the observed region was calculated. Each value from the mutant mice was normalized to the wild-type mouse. Statistical analysis was done using a Student's *t*-test. Graphs show mean ± SEM.

Video monitoring of mice

Video monitoring was conducted for $Arx^{PL/Y}$ mice at the onset of weaning (P1m) and at the adult age (P5–6m) and for $Arx^{(GCG)7/Y}$ mice at P1m (each $n = 10$) in their home cages. The room light was on from 8:00 a.m. to 8:00 a.m., and their behavior was monitored with a CCD camera during the dark period (9–11 h/day) for 4 days under infrared light illumination. The data were stored in a hard disk recorder, and convulsive behavior was checked off-line by viewing the animals' behavior on a screen.

Surface and depth EEG recording

$Arx^{PL/Y}$ and $Arx^{(GCG)7/Y}$ mice and their wild-type littermates ($n = 3$ for each group) at P39–49 (P1m) were used for EEG recordings. Under chloral hydrate anesthesia (400 mg/kg, i.p.), four stainless wire electrodes (200 μm in diameter) were implanted using a stereotaxic apparatus (SR-8N, Narishige, Japan). One electrode was placed on the dura at

the frontal cortex (F-cx; AP +1.0, L 2.0 from the Bregma; 51). Two wire electrodes were placed in the dorsal (Str-u; AP +1.0, L 2.0, DV 3.0) and ventral (Str-l; DV 4.0) parts of the striatum. Another wire electrode was inserted into the hippocampus (Hip; AP −2.0, L 2.0 DV 2.0) (Fig. 3B1 and B2). The reference screw electrode was placed on the cerebellum surface. Lead wires from the electrodes were connected to a socket. And the electrodes and the socket were firmly attached to the skull with acrylic resin cement. After a recovery period of 3 days after surgery, an EEG was recorded for 1–2 days in a sound-attenuated experimental box. The data were amplified 1000 times (time constant; 0.1 s, low-pass filter; 100 Hz, AB-621G, Nihon Kohden, Japan) and monitored on a computer screen (Spike2 ver. 5, Cambridge Electronics Design, UK). The behavior of the mice was monitored with a CCD camera in the experimental box and recorded using a digital video camera (DCR-DVD301, Sony, Japan). The behavioral changes and accompanying EEG data were checked offline. After the experiments, electrode positions were verified histologically (Fig. 3B).

Bicuculline treatment

To determine the seizure threshold and its change with age, $Arx^{PL/Y}$ and $Arx^{X/Y}$ mice at P1m (each $n = 6$) and P3–5m (each $n = 8$) received subcutaneous injections of 1.5 mg/kg bicuculline and their convulsive behavior was monitored for 30 min. The number of mice displaying myoclonic jerks and generalized seizures was recorded. In addition, the onset times of the first jerk and the first generalized seizure and the time of death from injection were recorded. Statistical differences in the number of mice and the time between injection and epileptic events were analyzed by Fisher's exact test and Mann–Whitney's *U*-test, respectively.

Experimental design for behavioral testing

The following behavioral tests were performed using $Arx^{PL/Y}$, $Arx^{(GCG)7/Y}$ and $Arx^{X/Y}$ mice backcrossed to a C57BL/6J genetic background for F8–F9 generations: the wire-hanging test (Supplementary Material, Fig. S3), the rotarod test (Supplementary Material, Fig. S3), the open-field test (Supplementary Material, Fig. S3), the step-through passive avoidance test (Fig. 4), the light–dark transition test (Supplementary Material, Fig. S4) and two divided tasks on the eight-arm radial maze including the win-shift task and the win-stay task (Fig. 4). After weaning around post-natal week 4 (post-natal day 26–29), the mice were housed two to five animals to a cage in a room with a 12 h light/dark cycle (light beginning at 8:00 a.m.) with ad libitum access to food and water, except during the eight-arm radial maze tests. Behavioral testing began after three nights and was performed between 9:00 a.m. and 7:00 p.m. Almost all behavioral tests were carried out using identical mice. The $Arx^{(GCG)7/Y}$ mice had a short lifespan and were almost all deceased by 10 weeks of age. To avoid a decrease in the number of mice tested due to death, the two tasks on the radial maze were separated from the other tests and were begun as soon as possible after weaning.

Step-through passive avoidance

The step-through passive avoidance test was performed over 2 days using the testing apparatus (O'Hara & Co. Tokyo) as described by Karl *et al.* (53). On day 1, the mouse was placed into the illuminated chamber facing the door to the darkened chamber. The door then opened, and the latency of entry to the darkened chamber was measured. Electric shocks (0.2 mA) were delivered 3 s after the mouse entered. The mouse could freely escape from the darkened chamber with the door open and was allowed to explore these chambers for 60 s after the shocks. On day 2, the mouse was again placed into the illuminated chamber, and the latency of its entry to the darkened chamber was measured, with a 300 s cut-off time.

The win-shift task on the eight-arm radial maze

The win-shift task was performed in a manner similar to that described by Miyakawa *et al.* (54), using the eight-arm radial maze (O'Hara & Co.). The win-shift task was conducted during a habituation and training phase. Food deprivation (each mouse received only a 2.5–3.0 g pellet a day) began 3–4 days before the habituation phase. Over the 7 days of the habituation phase, the mouse underwent each of the three steps of pre-training in turn. In the first step, the mouse was allowed to freely explore the maze for 10 min without food reward. In the second and third steps, the protocol described by Miyakawa *et al.* (54) was followed. After the habituation phase, actual training began. All eight arms were baited with food pellets. The mouse was allowed to retrieve all eight pellets, with a 7 s confinement in the central platform before being presented with the next arm choice. The trial continued until the mouse had consumed all eight pellets or 10 min had elapsed. Training occurred once daily for 18 days. Image J RM software was used both to carry out the procedure and to analyze behavioral performance. Data for each mouse were averaged every three trials for statistical analysis.

The win-stay task on the eight-arm radial maze

The eight-arm radial maze was modified for the win-stay task. The eight arms had black opaque walls, and food dispensers were attached to the end of each arm to drop a sucrose pellet into the well. Light bulbs were set above the entrance to each arm facing the end of the arm. The apparatus was surrounded by a black curtain to restrict spatial cues and room light. The mice underwent the same food-deprivation schedule as in the win-shift task. The habituation and training phases were conducted for the win-stay task, during which four randomly selected arms were lit, but no more than three successive adjacent arms were lit on each trial. In the habituation phase, the mouse was allowed to freely explore the maze for 10 min a day for 3 days. The actual training was performed as described previously (55), following the habituation phase. A single pellet was placed in each well of the lit arms. The mouse was given two chances to retrieve the pellet in each lit arm and confined in the central platform for 7 s between each lit or unlit arm choice. This procedure was manually operated by remote control with video monitor-

ing. One trial per day continued until the mouse had consumed all eight pellets or 10 min had elapsed. The latency to consume all pellets and the number of lit or unlit arms visited were measured for each trial. Data for each animal were averaged every three trials for statistical analysis.

Collection of behavioral indices for the eight-arm radial maze for the $Arx^{(GCG)7/Y}$ mice

Behavioral indices were collected, except for trials in which total choices were fewer than eight, which came from the total choices when a mouse retrieved all eight pellets without incorrect arm choices, because irregular and abnormal behavior occurred so often that the mouse had difficulty turning and choosing an arm. Additionally, if we saw an epileptic seizure, we allowed a 30–60 min interval before a trial to let the mouse calm down. Trials were sometimes stopped when it was apparent that a mouse could not move without difficulty.

Image analysis and statistical analysis

Software used for the behavioral tests (Image J OF, Image J LD, Image J EP and Image J RM) was modified on the public domain Image J program, developed by the US National Institutes of Health (available through O'Hara & Co). Each behavioral index was compared between the *Arx* mutant mice and $Arx^{X/Y}$ mice nursed by the heterozygous dams with the same kind of mutant allele. The data were analyzed using a two-tailed Student's *t*-test or two-way RMANOVA, unless noted otherwise, using Excel or GraphPad Prism 5. Graphs show mean ± SEM.

SUPPLEMENTARY MATERIAL

Supplementary Material is available at *HMG* online.

ACKNOWLEDGEMENTS

The authors express their appreciation to E. Robertson for providing the CCE ES cells and V. Pachnis for the *Lhx8*; K. Omichi, E. Iida, Y. Motegi, T. Hino, S. Kumagai and A. Takahashi for their technical support and K. Wada and K. Inoue for their encouragement.

Conflict of Interest statement. None declared.

FUNDING

This study was supported in part by the Research Grants (15B-4, 18A-5 and 21B-6) for Nervous and Mental Disorders from the Ministry of Health, Labour and Welfare (YG), and grants from the Organization for Pharmaceutical Safety and Research (MP-J) and the Institute of Biomedical Innovation (05-41), Japan (YG).

REFERENCES

1. Miura, H., Yanazawa, M., Kato, K. and Kitamura, K. (1997) Expression of a novel *aristaless* related homeobox gene '*Arx*' in the vertebrate telencephalon, diencephalon and floor plate. *Mech. Dev.*, **65**, 99–109.
2. Ohira, R., Zhang, Y.H., Guo, W., Dipple, K., Shih, S.L., Doerr, J., Huang, B.L., Fu, L.J., Abu-Khalil, A., Geschwind, D. and McCabe, E.R.B. (2002) Human *ARX* gene: genomic characterization and expression. *Mol. Genet. Metab.*, **77**, 179–188.
3. Kitamura, K., Yanazawa, M., Sugiyama, N., Miura, H., Iizuka, A., Kusaka, M., Omichi, K., Suzuki, R., Kato-Fukui, Y., Kamiirisa, K. *et al.* (2002) Mutation of *ARX* causes abnormal development of forebrain and testes in mice and X-linked lissencephaly with abnormal genitalia in human. *Nat. Genet.*, **32**, 359–369.
4. Strφmme, P., Mangelsdorf, M.E., Shaw, M.A., Lower, K.M., Lewis, S.M.E., Bruyere, H., Luttcherath, V., Gedeon, A.G., Wallace, R.H., Scheffer, I.E. *et al.* (2002) Mutations in the human ortholog of Aristaless cause X-linked mental retardation and epilepsy. *Nat. Genet.*, **30**, 441–445.
5. Bienvenu, T., Poirier, K., Friocourt, G., Bahi, N., Beaumont, D., Faucheeau, F., Jeema, L.B., Zemni, R., Vinet, M-C., Francis, F. *et al.* (2002) *ARX*, a novel Prd-class-homeobox gene highly expressed in the telencephalon, is mutated in X-linked mental retardation. *Hum. Mol. Gen.*, **11**, 981–991.
6. Sherr, E.H. (2003) The *ARX* story (epilepsy, X-linked mental retardation, autism, and cerebral malformations): one gene leads many phenotypes. *Curr. Opin. Pediatr.*, **15**, 567–571.
7. Kato, M., Das, S., Petras, K., Kitamura, K., Morohashi, K., Abuelo, D., Barr, M., Bonneau, D., Brady, A., Carpenter, N. *et al.* (2004) Mutations of *ARX* are associated with striking pleiotropy and consistent genotype–phenotype correlation. *Hum. Mutat.*, **23**, 147–159.
8. Gecz, J., Cloosterman, D. and Partington, M. (2006) *Arx*: a gene all seasons. *Curr. Opin. Genet. Develop.*, **16**, 308–316.
9. Hirose, S. and Mitsudome, A. (2003) X-linked mental retardation and epilepsy: pathogenetic significance of *ARX* mutations. *Brain Dev.*, **25**, 161–163.
10. Collombat, P., Mansouri, A., Hecksher-Sorensen, J., Serup, P., Krull, J., Gradwohl, G. and Gruss, P. (2003) Opposing actions of Arx and Pax4 in endocrine pancreas development. *Genes Dev.*, **17**, 2591–2603.
11. Yoshihara, S., Omichi, K., Yanazawa, M., Kitamura, K. and Yoshihara, Y. (2005) *Arx* homeobox gene is essential for development of mouse olfactory system. *Development*, **132**, 751–762.
12. Biressi, S., Messina, G., Collombat, P., Tagliafico, E., Moteverde, S., Benedetti, L., Cusella De Angelis, M.G., Mansouri, A., Ferrari, S., Tajbakhsh, S., Broccoli, V. and Cossu, G. (2005) The homeobox gene Arx is a novel positive regulator of embryonic myogenesis. *Cell Death Differ.*, **15**, 94–104.
13. Poirier, K., Van Esch, H., Friocourt, G., Sailour, Y., Bahi, N., Backer, S., Souil, E., Castelnau-Ptakhine, L., Beldjord, C., Fransis, F., Bienvenu, T. and Chelly, J. (2004) Neuroanatomical distribution of ARX in brain and its localization in GABAergic neurons. *Brain Res. Mol. Brain Res.*, **122**, 35–46.
14. Friocourt, G., Poirier, K., Rakic, S., Parnavelas, J.G. and Chelly, J. (2006) The role of ARX in cortical development. *Eur. J. Neurosci.*, **23**, 869–876.
15. Colombo, E., Collombat, P., Colasante, G.M., Blanchi Long, J., Mansouri, A., Rubenstein, J.F.R. and Broccoli, V. (2007) Inactivation of Arx, the murine ortholog of the X-linked lissencephaly with ambiguous genitalia gene, leads to sever disorganization of the ventral telencephalon with impaired neuronal migration and differentiation. *J. Neurosci.*, **27**, 4786–4798.
16. Seufert, D.W., Prescott, N.L. and El-Hodiri, H.M. (2005) Xenopus aristaless related homeobox (*xARX*) gene product functions as both a transcriptional activator and repressor in forebrain development. *Dev. Dyn.*, **232**, 313–324.
17. Mckenzie, O., Ponte, I., Mangelsdorf, M., Finnis, M., Colasante, G., Shoubridge, C., Stifani, S., Gecz, J. and Broccoli, V. (2007) *Aristaless*-related homeobox gene, the responsible for West syndrome and related disorders, is a groucho/tranducilin-like enhancer of split dependent transcriptional repressor. *Neuroscience*, **146**, 236–247.
18. Cobos, I., Broccoli, V. and Rubenstein, J.L.R. (2005) The vertebrate of ortholog of *Aristaless* is regulated by *Dlx* genes in the developing forebrain. *J. Comp. Neurol.*, **483**, 292–303.

19. Fulp, C.T., Cho, G., Marsh, E.D., Nasrallah, I.M., Labosky, P.A. and Golden, J.A. (2008) Identification of Arx transcriptional targets in the developing basal forebrain. *Hum. Mol. Genet.*, **17**, 3740–3760.
20. Colasante, G., Collombat, P., Raimondi, V., Bonanomi, D., Ferrai, C., Maira, M., Yoshikawa, K., Mansouri, A., Valtorta, F., Rubenstein, J.L. and Broccoli, V. (2008) Arx is a direct target of Dlx2 and thereby contributes to the tangential migration of GABAergic interneurons. *J Neurosci.*, **28**, 10674–10686.
21. Tamamaki, N., Yanagawa, Y., Tomioka, R., Miyazaki, J., Obata, K. and Knaeko, T. (2003) Green fluorescent protein expression and colocalization with calretinin, paralbumin, and somatostain in the GSAD67-GFP knock-in mouse. *J. Comp. Neurol.*, **467**, 60–79.
22. Tanaka, D.H., Maekawa, K., Yanagawa, Y., Obata, K. and Murakami, F. (2006) Multidirectional and multizonal migration of GABAergic interneurons in the developing cerebral cortex. *Development*, **133**, 2167–2176.
23. Hevner, R.F., Shi, L., Justice, N., Hsueh, Y.-P., Sheng, M., Smiga, S., Bulfone, A., Goffinet, A.M., Campagnoni, A.T. and Rubenstein, J.L.R. (2001) Tbr1 regulates differentiation of the preplate and layer 6. *Neuron*, **29**, 353–366.
24. Ferland, R.J., Cherry, T.J., Preware, P.O., Morrisey, E.E. and Walsh, C.A. (2003) Characterization of Foxp2 and Foxp1 mRNA and protein in the developing and mature brain. *J. Comp. Neurol.*, **460**, 266–279.
25. Britanova, O., Romero, C.J., Cheung, A., Kwan, K.Y., Schwark, M., Gyorgy, A., Vogel, T., Akopov, S., Mitkovski, M., Agoston, D. *et al.* (2008) Satb2 is a postmitotic determinant for upper-layer neuron specification in the neocortex. *Neuron*, **57**, 378–392.
26. Bonneau, D., Toutain, A., Laguerriere, A., Marret, S., Saugier-Veber, P., Barthez, M.A., Radi, S., Biran-Mucignat, V., Rodriguez, D. and Gélot, A. (2002) X-linked lissencephaly with absent corpus callosum and ambiguous genitalia (XLAG): clinical, magnetic resonance imaging, and neuropathological findings. *Ann. Neurol.*, **51**, 340–349.
27. Okazaki, S., Ohsawa, M., Kuki, I., Kawasaki, H., Koriyama, T., Ri, S., Ichiba, H., Hai, E., Inoue, T., Nakamura, H. *et al.* (2008) *Aristaless*-related homeobox gene disruption leads to abnormal distribution of GABAergic interneurons in the human neocortex: evidence based on a case of X-linked lissencephaly with abnormal genitalia (XLAG). *Acta Neuropathol.*, **116**, 453–462.
28. Nasrallah, I.M., Minarcik, J.C. and Golden, J.A. (2004) A polyalanine tract expansion in ARX forms intranuclear inclusions and results in increased cell death. *J. Cell Biol.*, **167**, 411–416.
29. Shoubridge, C., Cloosterman, D., Parkinson-Lawerence, E., Brooks, D. and Gecz, J. (2007) Molecular pathology of expanded polyalanine tract mutations in the *Aristaless*-related homeobox gene. *Genomics*, **90**, 59–71.
30. Forman, M.S., Squier, W., Dobyns, W.B. and Golden, J.A. (2006) Genotypically defined lissencephalies show distinct pathologies. *J. Neuropathol. Exp. Neurol.*, **64**, 847–857.
31. Friocourt, G., Kanatani, S., Tabata, H., Yozu, M., Takahashi, T., Antypa, M., Raguenes, O., Chelly, J., Ferec, C., Nakajima, K. and Parnavelas, J.G. (2008) Cell-autonomous roles of ARX in cell proliferation and neuronal migration during corticogenesis. *J. Neurosci.*, **28**, 5794–5705.
32. Wilson, D.S., Sheng, G., Jun, S. and Desplan, C. (1996) Conservation and diversification in homeodomain-DNA interactions: a comparative genetic analysis. *Proc. Natl Acad. Sci. USA*, **93**, 6886–6891.
33. Lacey, J.C. Jr and Pruitt, K.M. (1996) Origin of the genetic code. *Nature*, **223**, 799–804.
34. Powell, E.M., Campbell, D.B., Stanwood, G.D., Davis, C., Noebels, J.L. and Levitt, P. (2003) Genetic disruption of cortical interneuron development causes region- and GABA cell type-specific deficits, epilepsy, and behavioral dysfunction. *J. Neurosci.*, **23**, 622–631.
35. Cobos, I., Elisa, M., Calcagnotto, E., Vilaythong, A.J., Thwin, M.T., Noebel, J.L., Baraban, S.C. and Rubenstein, J.L.R. (2005) Mice lacking *Dlx1* show subtype-specific loss of interneurons, reduce inhibition and epilepsy. *Nat. Neurosci.*, **8**, 1059–1063.
36. Freund, T.F. and Antal, M. (1988) GABA-containing neurons in the septum control inhibitory interneurons in the hippocampus. *Nature*, **336**, 170–173.
37. Frotscher, M. and Léránth, C. (1985) Cholinergic innervation of the rat hippocampus as revealed by choline acetyltransferase immunocytochemistry: a combined light and electron microscopic study. *J. Comp. Neurol.*, **225**, 327–343.
38. Ferencz, I., Leanza, G., Nanobashvili, A., Kokaia, Z., Kokaia, M. and Lindvall, O. (2001) Septal cholinergic neurons suppress seizure development in hippocampal kindling in rats: comparison with noradrenergic neurons. *Neuroscience*, **102**, 819–832.
39. Butuzova, M.V. and Kitchigina, V.F. (2008) Repeated blockade of GABAA receptors in the medial septal region induces epileptiform activity in the hippocampus. *Neurosci. Lett.*, **434**, 133–138.
40. An, J.J., Bae, M.H., Cho, S.R., Lee, S.H., Choi, S.H., Lee, B.H., Shin, H.S., Kim, Y.N., Park, K.W., Borrelli, E. and Baik, J.H. (2004) Altered GABAergic neurotransmission in mice lacking dopamine D2 receptors. *Mol. Cell. Neurosci.*, **25**, 732–741.
41. Liu, Q., Han, D., Wang, S. and Zou, Z.Y. (2005) Characteristic neuronal firing interspike intervals in laterodorsal thalamic nuclei induced by tetanization of rat caudate putamen: possible relations to hippocampal electroencephalogram changes. *Acta Physiologica Sinica*, **25**, 573–586.
42. Bracci, E., Centonze, D., Bernardi, G. and Calabresi, P. (2004) Engagement of rat striatal neurons by cortical epileptiform activity investigated with paired recordings. *J. Nuerophysiol.*, **92**, 2725–2737.
43. Wu, J.F., Han, D., Hu, L. and Zou, Z.Y. (2006) Contralateral 80–280 Hz EEG ripples and hippocampal single unit discharge inhibition in response to acute tetanization of rat right caudate putamen *in vivo*. *Epilepsy Res.*, **70**, 59–72.
44. Myhrer, T. (2003) Neurotransmitter systems involved in learning and memory in the rat: a meta-analysis based on studies of four behavioral tasks. *Brain Res. Brain Res. Rev.*, **41**, 268–287.
45. McDonald, R.J. and White, N.M. (1993) A triple dissociation of memory systems: hippocampus, amygdala, and dorsal striatum. *Behav. Neurosci.*, **107**, 3–22.
46. Parent, M.B. and Baxter, M.G. (2004) Septohippocampal acetylcholine: involved in but not necessary for learning and memory? *Learn. Mem.*, **11**, 9–20.
47. Fuchs, E.C., Zivkovic, A.R., Cunningham, M.O., Middleton, S., Lebeau, F.E., Bannerman, D.M., Rozov, A., Whittington, M.A., Traub, R.D., Rawlins, J.N. and Monyer, H. (2007) Recruitment of parvalbumin-positive interneurons determines hippocampal function and associated behavior. *Neuron*, **53**, 591–604.
48. Tepper, J.M. and Bolam, J.P. (2004) Functional diversity and specificity of neostriatal interneurons. *Curr. Opin. Neurobiol.*, **14**, 685–692.
49. Kitabatake, Y., Hikida, T., Watanabe, D., Pastan, I. and Nakanishi, S. (2003) Impairment of reward-related learning by cholinergic cell ablation in the striatum. *Proc. Natl Acad. Sci. USA*, **100**, 7965–7970.
50. Ehninger, D., Li, W., Fox, K., Stryker, M.P. and Silva, A.J. (2008) Reversing neurodevelopmental disorders in adults. *Neuron*, **60**, 950–960.
51. Paxions, G. and Franklin, K.B.J. (1997) *The Mouse Brain*. Academic Press, New York.
52. Fragkouli, A., Hean, C., Errington, M., Cooke, S., Grigoriou, M., Bliss, T., Stylianopoulou, F. and Pachnis, V. (2005) Loss of forebrain cholinergic neurons and impairment in spatial leaning and memory in LHX7-deficient mice. *Eur. J. Nurosci.*, **21**, 2923–2938.
53. Karl, T., Pabst, R. and von Hörsten, S. (2003) Behavioral phenotyping of mice in pharmacological and toxicological research. *Exp. Toxicol. Pathol.*, **55**, 69–83.
54. Miyakawa, T., Yamada, M., Duttaroy, A. and Wess, J. (2001) Hyperactivity and intact hippocampus-dependent learning in mice lacking the M1 muscarinic acetylcholine receptor. *J. Neurosci.*, **21**, 5239–5250.
55. Robert, J.M. and Morman, N.M. (1993) A triple dissociation of memory systems: hippocampus, amygdala, and dorsal striatum. *Behav. Neuro.*, **107**, 3–32.

Gene 432 (2009) 60–66

Contents lists available at ScienceDirect

Gene

journal homepage: www.elsevier.com/locate/gene

Molecular cloning and characterization of the common marmoset huntingtin gene

Hirohiko Hohjoh [a,*], Hirofumi Akari [b], Yuko Fujiwara [a,c], Yoshiko Tamura [a], Hirohisa Hirai [d], Keiji Wada [c]

[a] Department of Molecular Genetics, National Institute of Neuroscience, NCNP, 4-1-1 Ogawahigashi, Kodaira, Tokyo 187-8502, Japan
[b] Laboratory of Disease Control, Tsukuba Primate Research Center, National Institute of Biomedical Innovation, Tsukuba, Ibaraki, Japan
[c] Department of Degenerative Neurological Diseases, National Institute of Neuroscience, NCNP, Kodaira, Tokyo, Japan
[d] Primate Research Institute, Kyoto University, Inuyama, Aichi, Japan

ARTICLE INFO

Article history:
Received 24 July 2008
Received in revised form 4 November 2008
Accepted 5 November 2008
Available online 24 November 2008

Received by M. Di Giulio

Keywords:
Common marmoset
Huntingtin
Gene silencing
Immortalized cell line

ABSTRACT

We report here for the first time the isolation and identification of the common marmoset (*Callithrix jacchus*) *huntingtin* (*Htt*) gene, whose ortholog in humans is known to be related to Huntington's disease (HD). A 9396 nucleotide complementary DNA (cDNA) carrying the putative full-length open reading frame of the marmoset *Htt* gene was identified, and highly conserved nucleotide and amino acid sequences among primates were observed. Based on this data and using tools evaluated for the detection of the marmoset *Htt* gene, we have demonstrated gene silencing against the expression of endogenous *Htt* gene in immortalized common marmoset mononuclear cells by means of RNA interference (RNAi). Taken together, the data presented here may assist us in realizing a non-human primate HD model with the common marmoset.

1. Introduction

Huntington's disease (HD) is an autosomal dominant neurodegenerative disease characterized by progressive and selective neural cell death associated with choreic movement and dementia (Walker, 2007). The responsible gene for HD, the huntingtin (Htt) gene, has been identified on chromosome 4q16.3 (Gusella et al., 1983; Gilliam et al., 1987), and an aberrant length of a CAG triplet repeat in exon 1, followed by expanded tracts of polyglutamine in the Htt polypeptide, is greatly involved in the onset of HD (Huntington's-Disease, 1993). Although the molecular mechanisms of either normal or aberrant Htt protein are still poorly understood, HD model animals (Mangiarini et al., 1996; Kazemi-Esfarjani and Benzer, 2000; von Horsten et al., 2003) and cells (Lunkes and Mandel, 1998) for understanding the pathogenesis of HD and developing therapies have been established by means of genetic engineering based on the genetic information of *Htt*. The use of an animal model that is closely related to humans may be particularly promising.

The common marmoset (*Callithrix jacchus*) is classified into the Callitrichidae family of Platyrrini (New World monkeys) and has been used as a non-human primate experimental animal in various research fields including gene therapy, autoimmune disease, organ transplantation, and pharmacology (Kendall et al., 1998; Doods et al., 2000; Deisboeck et al., 2003; t'Hart et al., 2003). Accordingly, it is worth promoting studies with the common marmoset aimed at overcoming neurodegenerative diseases such as HD, as the animal's close relationship to humans makes it well suited to this kind of study. Indeed, a recent study has generated a non-human primate HD model with the rhesus monkey (*Macaca mulatta*) (Palfi et al., 2007; Yang et al., 2008).

In this report, we describe for the first time the isolation and characterization of a cDNA encoding the putative full-length open reading frame of the common marmoset *Htt* gene, and present experimental data based on the isolated cDNA. The data presented here may provide us with useful information for establishing non-human primate HD models with the common marmoset.

2. Materials and methods

2.1. Preparation of total RNA

Common marmoset total RNA was isolated from the brain tissue of a stillborn marmoset fetus and immortalized monocytes (described below) using Trizol (Invitrogen). The experiments with the common marmoset complied with protocols approved by the ethical committee for primate research of the National Center of Neurology and Psychiatry and adhered to the legal requirements of Japan.

Abbreviations: HD, Huntington's disease; Htt, huntingtn; RNAi, RNA interference; cDNA, complementary DNA; PBMC, peripheral blood mononuclear cell; RT, reverse transcription; PCR, polymerase chain reaction; ORF, open reading frame; APP, amyloid precursor protein; GAPDH, glyceraldehyde-3-phosphate dehydrogenase; GFP, green fluorescence protein; CMV, Cytomegalovirus.

* Corresponding author.
E-mail address: hohjohh@ncnp.go.jp (H. Hohjoh).

0378-1119/$ – see front matter © 2008 Elsevier B.V. All rights reserved.
doi:10.1016/j.gene.2008.11.012

2.2. Established common marmoset cell lines

Adult common marmosets being reared at the Primate Research Institute of Kyoto University or Tsukuba Primate Research Center were anesthetized by ketamine, which was approved by the Animal Welfare and Animal Care Committees of both institutes, and peripheral blood was collected. From the collected blood samples, peripheral blood mononuclear cells (PBMCs) were purified and immortalized by infection of a 488-77 strain of *Herpesvirus saimiri* (kindly provided by Dr. R. C. Desrosiers) as previously described (Akari et al., 1996). The established marmoset cell lines, designated HSCj-110, HSCj-009, and HSCj-002, were phenotypically activated CD3+T lymphocytic cells and grown in RPMI-1640 medium (Sigma) supplemented with 10% FCS, 50 mM 2-mercaptoethanol, and antibiotics.

2.3. Reverse transcription – (real time) polymerase chain reaction [RT-(real time) PCR]

The common marmoset total RNAs were subjected to complementary DNA (cDNA) synthesis using oligo(dT) primers and a Superscript III reverse transcriptase (Invitrogen), according to the manufacturer's instructions, and polymerase chain reaction (PCR) using the cDNAs as templates was carried out by means of the ABI GeneAmp PCR system 9700 (Applied Biosystems). In the case of real time PCR, the cDNAs were examined by the AB 7300 Real Time PCR System (Applied Biosystems) with a TaqMan Universal PCR Master Mix together with Assays-on-Demand Gene Expression products (Applied Biosystems) or a SYBR Green PCR Master Mix together with Perfect Real Time Primers (Takara Bio) or designed PCR primers, according to the manufacturers' instructions. Synthesized oligonucleotide primers and purchased primer and probe were as follows:

Synthesized oligonucleotide primers:

HD1-F: 5′-TATAGAATTCGGGAGACCGCCATGGCGAC-3′
HD1-ORF-R: 5′-TCAAGCGGCCGCTCAGCAGGTGGTGACCTTG-3′
HD1-1900R2: 5′-TAAAGGATCCCCGTCTAACACAATTTCAG-3′
cjHtt(1139)-F: 5′-TTATAGCTGGAGGCGGTTCC-3′
cjHtt(1254)-R: 5′-GACGTCCGACCTCGATTCAG-3′

Purchased primer and probe:

Assays-on-Demand Gene Expression product for the human *Htt* gene (Assay ID: Hs00169273_m1) (Applied Biosystems).

Perfect Real Time Primers for the human *GAPDH* gene (Primer-Set ID: HA067812) (Takara Bio).

2.4. Cloning and sequence analysis of the full-length ORF of the marmoset Htt gene

Complementary DNA derived from the common marmoset total RNA was subjected to PCR amplification using *TaKaRa LA Taq* polymerase (TAKARA BIO) with the HD1-F and HD1-ORF-R primers under the following thermal cycling conditions: heat denaturation at 94 °C for 1 min, 30 cycles of amplification including denaturation at 94 °C for 20 s and extension at 68 °C for 12 min, and a final extension at 72 °C for 10 min. The PCR product was examined by agarose gel electrophoresis followed by ethidium bromide staining, and an approximately 9.4 kb PCR band (Fig. 1) was purified from the gels using a TOPO XL gel purification kit (Invitrogen). The resultant PCR product was inserted into the pCR-XL-TOPO plasmid with a TOPO XL PCR cloning kit (Invitrogen) and then sequence determination of the insert was carried out. To clarify uncertain nucleotide sequences, additional RT-PCR targeting of uncertain regions followed by sequence determination was performed and the precise nucleotide sequence was confirmed. The determined nucleotide sequence encoding a putative full-length ORF of the common marmoset *Htt* gene has been registered in the GenBank database: accession number, AB443866.

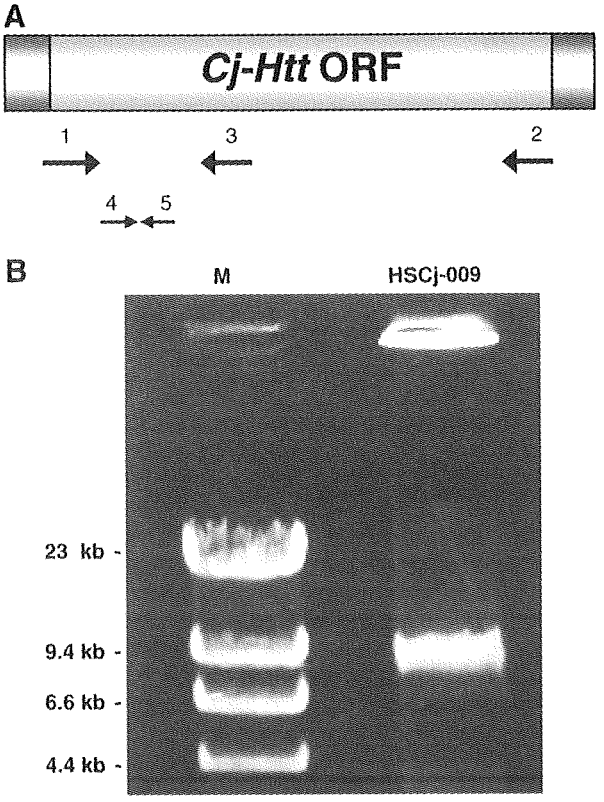

Fig. 1. RT-PCR amplification. (A) Schematic drawing of putative *Htt* cDNA. Open reading frame (ORF) is indicated by a yellow box. Arrows indicate synthesized PCR primers, which are designed in possibly conserved nucleotide sequences: 1, HD1-F; 2, HD1-ORF-R; 3, HD1-1900R2; 4, cjHtt(1139)-F; 5, cjHtt(1254)-R (detailed in Materials and methods). (B) RT-PCR. The first strand cDNA was synthesized by RT using RNA isolated from immortalized common marmoset mononuclear cells (HSCj-009) as a template and oligo(dT) as a primer. The following PCR was carried out using HD1-F and HD1-ORF-R primers. The resultant PCR products were analyzed by gel electrophoresis with 0.6 % agarose gel followed by ethidium bromide staining. Hind III-digested λDNA was used as a DNA size marker (M).

2.5. Western blotting

Equal amounts (~35 μg) of protein extracts from the common marmoset and mouse brain tissues and established PBMC lines (described above) were separated by SDS-PAGE with 5% polyacrylamide gels and electrophoretically blotted onto PVDF membranes (Millipore). Membranes were blocked for 1 h in blocking solution [5% non-fat milk in TBST buffer (25 mM Tris-HCl, pH 7.4, 150 mM NaCl and 0.1% Tween-20)] and incubated with 1/1000 dilution of mouse anti-huntingtin protein monoclonal antibodies [MAB2166 and MAB2170 (Chemicon); ab7666 (Abcam)] followed by washing in TBST buffer and further incubation with sheep anti-mouse Ig, HRP-linked whole Ab (GE Healthcare). Antigen-antibody complexes were visualized using ECL plus Western Blotting Detection Reagent (GE Healthcare). After detection of signals, the membranes were subjected to antibody removal in Re-Blot Plus strong antibody stripping solution (Chemicon) followed by washing in TBST buffer, and then incubated with 1/1000 dilution of mouse anti-APP [MAB348 (Chemicon)] monoclonal antibody. Subsequent processes were the same as described above.

2.6. Gene silencing of marmoset Htt by RNA interference

To monitor gene silencing against the common marmoset *Htt* gene, we constructed a reporter plasmid carrying the 5′-terminal region of the marmoset *Htt* linked with the *GFP* reporter gene: the PCR product obtained from RT-PCR with the HD1-F and HD1-1900R2 primers was

Table 1
Sequence homologies (%) among various species' *Htt* genes

Homo sapiens	*Callithrix jacchus*	*Canis lupus familiaris*	*Bos taurus*	*Sus scrofa*	*Mus musclus*	*Rattus norvegicus*
Homo sapiens	**95.1** **97.0**	87.0 92.0	84.0 89.5	84.1 88.6	86.1 91.2	85.8 91.2
Canis lupus familiaris		86.6 91.4	84.0 88.4	83.9 87.9	85.6 90.8	85.1 90.9
Callithrix jacchus			84.5 89.4	84.4 89.7	84.0 89.2	83.8 89.3
Bos taurus				86.8 89.3	81.2 87.1	81.3 87.4
Sus scrofa					80.9 86.9	80.8 87.2
Mus musclus						95.9 97.6
Rattus norvegicus						

Figures in upper and lower stands represent nucleotide and amino acid sequence homologies, respectively, between two species.

trimmed with EcoRI and BamHI, and inserted into the pd2EGFP-N1 plasmid (Clontech) treated with the same restriction enzymes. The resultant reporter (5′*Cj-Htt-GFP*) plasmid and synthetic siRNA duplex targeting the marmoset *Htt* (cjHtt-1 siRNA duplex) were cotransfected into mouse neuroblastoma Neuro2a cells by Lipofectamine 2000 transfection reagent (Invitrogen) as described previously (Sakai and Hohjoh, 2006). Two days after transfection, the cells were examined by a fluorescent microscope. When the endogenous marmoset *Htt* gene was inhibited by RNAi, the cjHtt-1 siRNA duplex (0.4 nmol/transfection) was introduced into HSCj-009 cells (1×10^6 cells/transfection) by means of a Nucleofector system (Amaxa Biosystems) according to the manufacturer's instructions. Two days after transfection, total RNA and cell lysate were prepared from the cells and examined by RT-real time PCR and Western blotting, respectively.

The nucleotide sequences of synthesized cjHtt-1 siRNA were as follows:

Sense: 5′-GCCUUUGAGUCCCUCAAGUUU-3′
Antisense: 5′-ACUUGAGGGACUCAAAGGCUU-3′

2.7. Sequence data and computational analyses

The *Htt* sequnece data derived from various species were as follows [GenBank accession number]: human (*Homo sapiens*) [NM_002111]; chimp (*Pan troglodytes*) [XM_517080]; rhesus macaque (*Macaca mulatta*) [XM_001086119]; canine (*Canis lupus familiaris*) [XM_536221]; bovine (*Bos taurus*) [XM_866758]; wild boar (*Sus scrofa*) [NM_213964]; mouse (*Mus musclus*) [NM_010414]; rat (*Rattus norvegicus*) [XM_573634]; chicken (*Gallus gallus*) [XM_420822]. Although the rhesus macaque Htt sequence [XM_001086119] contains 20 undetermined nuclotides at positons 4932–4951 followed by 6 suspensive amino acid sequences, the sequence was used and examined together with the other sequneces in this study.

Sequence homology analysis of either nucleotide or amino acid sequences was carried out by means of the GENETYX software (Software Development Co., Ltd., Tokyo, Japan), where all the parameters were set at default. For identification of the HEAT repeats in the Cj-Htt protein sequences, the REP program (http://www.embl-heidelberg.de/~andrade/papers/rep/search.html) developed by Andrade et al. was used.

3. Results and discussion

3.1. Isolation and characterization of the common marmoset Htt gene

To isolate and identify the common marmoset *Htt* (*Cj-Htt*) gene and/or gene products, we focused on conserved regions in the *Htt* gene and isolate cDNA clone of the *Cj-Htt* transcript. Highly homologous regions (sequences) between the human and mouse *Htt* genes, whose corresponding regions in the *Cj-Htt* gene were also expected to remain conserved, were selected, and PCR primers were designed for such regions. We add that such conserved regions are also detectable by BLAST search with the human *Htt* as a query on the Trace archive of the Cj-database in NCBI. RT-PCR with the designed primers and total RNA extracted from common marmoset brain tissue and established cell lines was carried out, and an approximately 9.4 kb long PCR product, which was expected to contain the full-length open reading frame (ORF) of *Cj-Htt*, was obtained (Fig. 1). The PCR product was subjected to sequence determination and then compared with various species' *Htt* genes. From the results, it was clear that the PCR product, which is 9396 nucleotides in length, was derived from the common marmoset *Htt* gene which encodes a predicted 3131 amino acid long Cj-Htt polypeptide (the sequence accession number in GenBank is AB443866). Sequence homologies in the *Htt* gene among various species are indicated in Table 1. From the data, it appears that both the nucleotide and predicted amino acid sequences of the *Cj-Htt*

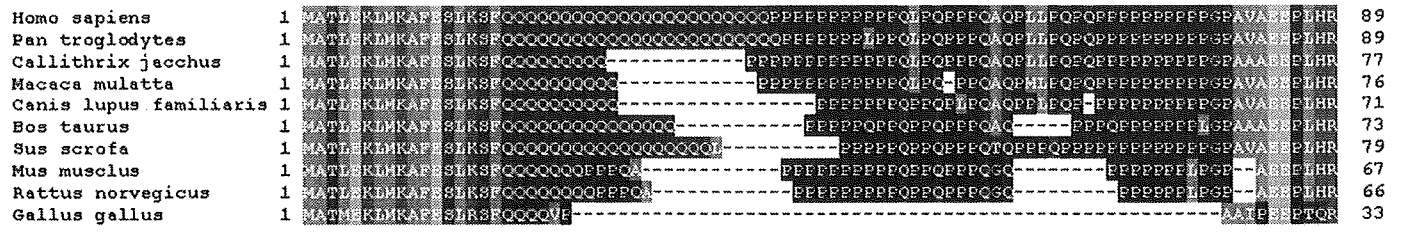

Fig. 2. Alignment of amino acid sequences in the Htt exon 1 and its corresponding regions. Sequence data were aligned based on the human Htt exon 1 (top line). Amino acid residues are color-coded based on the biochemical properties of the residues: hydrophobic amino acids in orange, polar amino acids with uncharged R groups in green, acidic amino acids in pink, basic amino acids in light blue, and special amino acids in dark blue.

Table 2
Alignment of HEAT repeats

Repeat*	Species**	AA position		Fragment†	Score	E-value
		From	To			
HEAT_AAA	Hs – Htt	124	162	QKLLGIAMELFLLCSDDAESDVRMVADECLNKVIKALMD	1510	1.26E-06
	Cj – Htt	112	150	QKLLGIAMELLLLCSDDAESDVRMVADECLNKVIKALMD	1590	5.48E-07
HEAT_AAA	Hs – Htt	205	243	RPYLVNLLPCLTRTSKRPEESVQETLAAAVPKIMASFGN	1990	1.03E-04
	Cj – Htt	193	231	RPYLVNLLPCLTRTSKRPEESVQETLAAAVPKIMASFGN	1990	2.37E-08
HEAT_AAA	Hs – Htt	247	285	DNEIKVLLKAFIANLKSSSPTIRRTAAGSAVSICQHSRR	1590	5.48E-07
	Cj – Htt	235	273	DNEIKILLKAFIANLKSSSPTIRRTAAGSAVSICQHSRR	1590	1.97E-06
HEAT_AAA	Hs – Htt	317	355	LLTLRYLVPLLQQQVKDTSLKGSFGVTRKEMEVSPSAEQ	1620	1.11E-06
	Cj – Htt	305	343	LLTLRYLVPLLHQQVKDTSLKGSFGVTRKEMEVSPSAEQ	1570	1.46E-07
HEAT_ADB	Hs – Htt					
	Cj – Htt	734	771	YPEEQYVSDILNYIDHGDPQVRGATAILCGTLVCSILS	1450	3.29E-07
HEAT_AAA	Hs – Htt	803	841	TFSLADCIPLLRKTLKDESSVTCKLACTAVRNCVMSLCS	1500	5.78E-07
	Cj – Htt	791	829	TFSLADCVPLLRKTLKDESSVTCKLACTAVRHCVMSLCS	1449	2.90E-06
HEAT_AAA	Hs – Htt	904	942	KLQERVLNNVVIHLLGDEDPRVRHVAAASLIRLVPKLFY	1930	6.69E-08
	Cj – Htt	892	930	TLQERVLESVVIHLLGDEDPRVRHVAAASLIRLVPKLFY	2150	2.51E-05
HEAT_AAA	Hs – Htt	984	1025	RIYRGYNLLPSITDVTMENNLSRVIAAVSHELITSTTRALTF	1370	9.05E-06
	Cj – Htt	972	1013	RIYRGYNLLPSIIDVTMENNLSRVIAAVSHELITSTTRALTF	1410	2.71E-06
HEAT_AAA	Hs – Htt	1425	1463	RLFEPLVIKALKQYTTTTCVQLQKQVLDLLAQLVQLRVN	1370	5.62E-06
	Cj – Htt	1413	1451	RLFEPLVIKALKQYTTTTSVQLQKQVLDLLAQLVQLRVN	1580	3.20E-07
HEAT_AAA	Hs – Htt	2798	2836	DDTAKQLIPVISDYLLSNLKGIAHCVNIHSQQHVLVMCA	1430	3.51E-06
	Cj – Htt	2785	2823	DDTAKQLIPVISDYLLSSLKGLAHCVNTHSQQHVLVMCA	1430	3.29E-06

* HEAT_AAA and HEAT_ADB indicate subsets of HEAT repeats representing PP2A and adaptin families, respectively.
** Hs-Htt and Cj-Htt indicate the human and common marmoset Htt proteins, respectively.
†Amino acids which are different from the sequence of Hs-Htt are indicated in red.

cDNA have significant sequence homology to that of other species' *Htt* genes. In addition, it should be noted that *Htt* sequences between the human and common marmoset (colored in yellow in Table 1) appear to be particularly conserved as compared with sequence conservation within non-primate *Htt* genes, suggesting that the *Htt* gene is highly conserved in primates.

Fig. 2 shows the alignment of amino acid sequences encoded by *Htt* exon 1 and its corresponding region in various species. From the alignment, *Cj-Htt* appears to possess a short polyglutamine tract of nine glutamines compared with that of the human and chimpanzee *Htt* genes; but other than the polyglutamine tract, the exon 1 corresponding region in *Cj-Htt* exhibits high sequence homology to the human *Htt* exon 1. It is also interesting that polyproline region adjacent to the polyglutamine tract has differences between primates and non-primates: amino acid substitutions and deletions are observed, and the lack of the polyproline region in the *Gallus gallus Htt* exon 1 is particularly remarkable. These differences may influence folding and aggregation of the Htt protein, and might represent adaptive evolution of *Htt* to each species. The difference in the exon 1 among various species may provide us with a hint for understanding the expansion of the polyglutamine tract in Huntington's disease in human.

Other than the exon 1 region, we also investigated the HEAT repeats possessing tandem arrayed bihelical structure, which appear to wrap around target substrates (Andrade and Bork, 1995; Neuwald and Hirano, 2000), and found that the HEAT repeats are also conserved in the Cj-Htt protein (Table 2). In addition, it may be interesting that HEAT_ADB, a subset of HEAT repeats representing adaptin family, is present in Cj-Htt, but not in Hs-Htt.

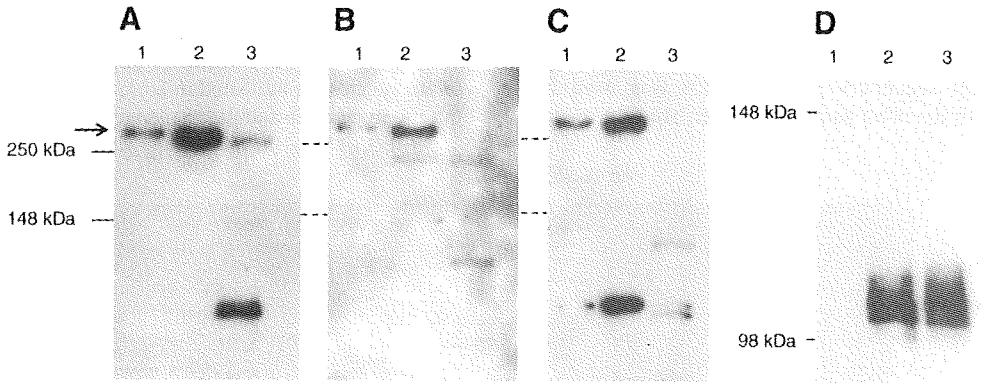

Fig. 3. Assessment of anti-human Htt antibodies against the common marmoset Htt polypeptide. Cell lysate derived from the common marmoset cell line (HSCj-110) (lane 1), brain tissue (lane 2), and mouse brain tissue as a control (lane 3) was examined by Western blotting with anti-human Htt antibodies. Tested antibodies were as follows: (A) MAB2166 (Chemicon), (B) MAB2170 (Chemicon), and (C) ab7666 (Abcam). Arrow indicates the signals of Htt proteins. The same results as those of HSCj-110 were also obtained when HSCj-002 and-009 were used (data not shown). After detection of signals, blotted membranes were subjected to antibody removal and then incubated with anti-APP antibody [MAB348 (Chemicon)] (D) followed by the same procedure as in the anti-human Htt antibodies described above.

3.2. Detection of Cj-Htt gene products

It is important to be able to properly detect the *Cj-Htt* gene and its gene products. Since the nucleotide and predicted amino acid sequences of the *Cj-Htt* cDNA showed significantly high sequence homologies to those of the human *Htt* gene, we tested whether commercially-available TaqMan probe and antibodies against human *Htt* gene products (mRNA and protein) were also able to detect *Cj-Htt* gene products. As a result, the TaqMan probe (Fig. 5A) appears to be able to detect *Cj-Htt* mRNA. In addition, newly designed PCR primers, which are perfectly matched to *Cj-Htt*, also appear to be able to detect *Cj-Htt* mRNA (Fig. 5B).

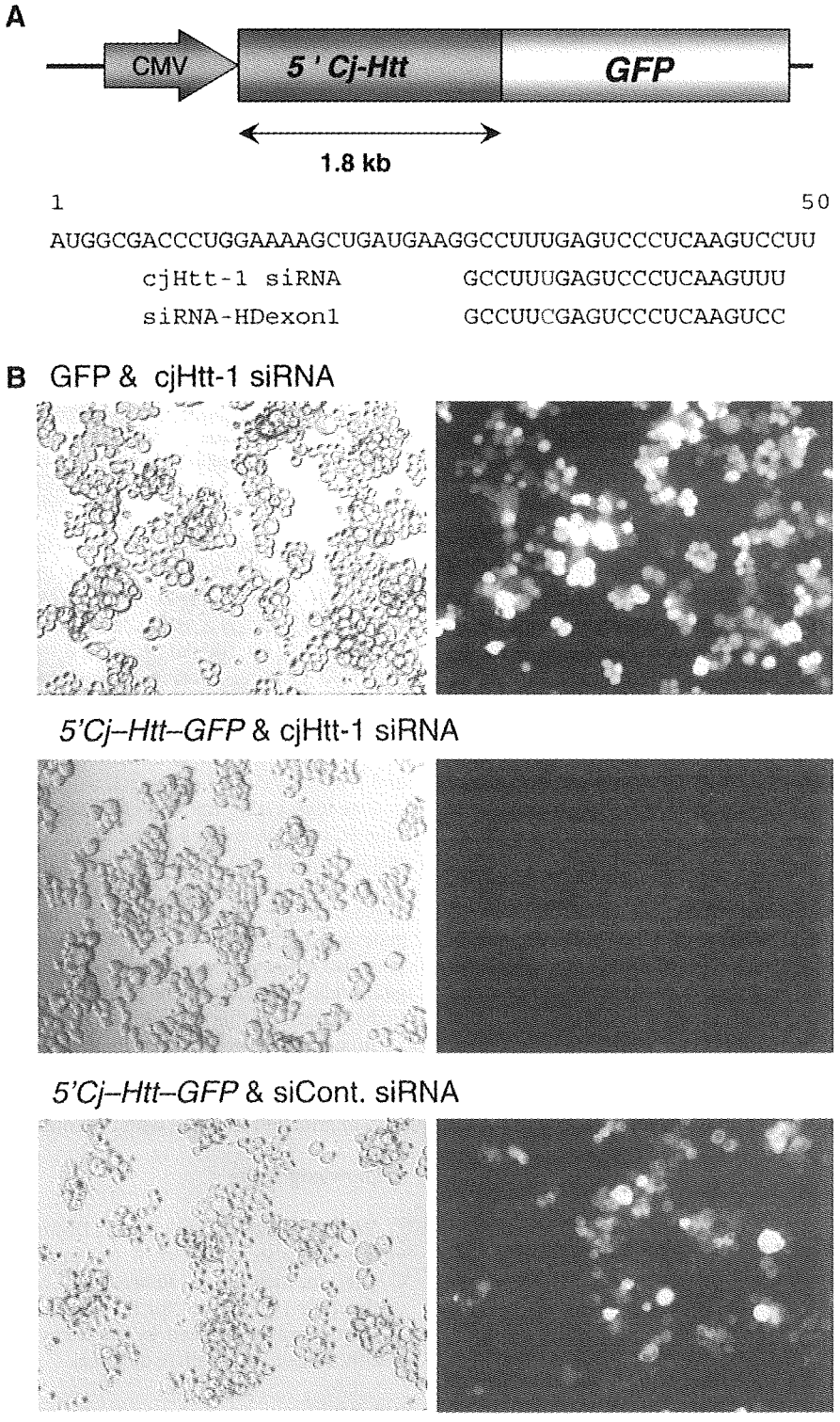

Fig. 4. Gene silencing against the 5′*Cj-Htt-GFP* fusion gene. (A) Schematic drawing of the 5′*Cj-Htt-GFP* fusion gene and designed cjHtt-1 siRNA. The fusion gene is composed of the 5′ terminal region of the Cj-Htt ORF and GFP, and driven by the Human cytomegalovirus promoter. The *Cj-Htt* sequence from the first ATG to position 50 is shown together with sequences of cjHtt-1 siRNA and siRNA-HDexon1 targeting human *Htt*. A variant nucleotide between the siRNAs is indicated in red. (B) Effect of cjHtt-1 siRNA on gene silencing. Reporter genes [5′*Cj-Htt-GFP* or *GFP* (empty reporter)] and siRNAs [cjHtt-1 or siCont (non-silencing siRNA)] were introduced into mouse neuroblastoma Neuro2a (N2a) cells. Two days after transfection, the cells were examined by a fluorescent microscope. Left (differential interference contrast) and right (fluorescence image) panels are identical in the visual field.

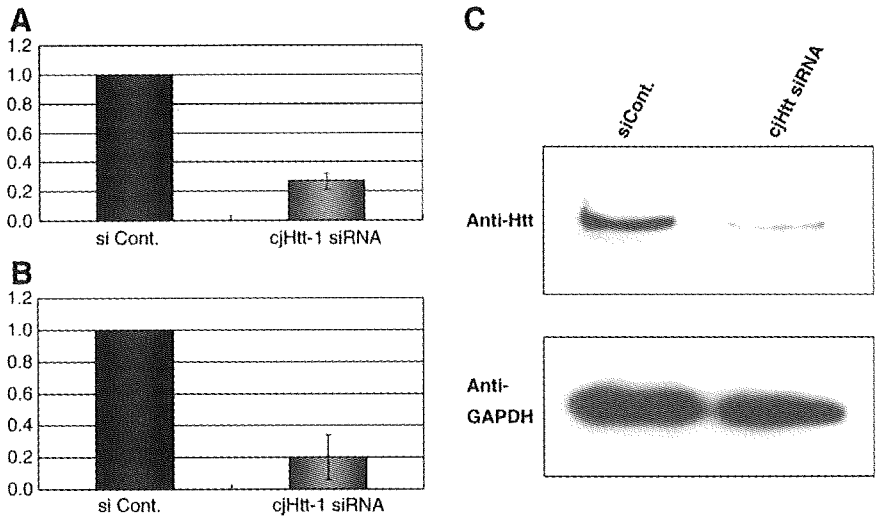

Fig. 5. Inhibition of expression of endogenous *Cj-Htt* by RNAi. The cjHtt-1 siRNA was introduced into HSCj-009 cells by means of electroporation. Two days after transfection, total RNA and cell lysate were prepared and examined by RT-real time PCR and Western blotting, respectively. Total RNA was subjected to cDNA synthesis as in Fig. 1. The resultant cDNA was examined by real time PCR with a TaqMan probe for the human *Htt* gene (A) and newly designed PCR primers [cjHtt(1139)-F and cjHtt(1254)-R] (B). The expression of *Gapdh* as a control was also examined using Perfect Real Time Primers for the human *GAPDH* gene (TAKARA BIO). The expression level of *Cj-Htt* was normalized against that of *Gapdh*, and the ratios of *Cj-Htt* expression level in the presence of cjHtt-1 siRNA were normalized against the ratio obtained in the presence of the siControl siRNA (siCont.). Data are means of at least three independent determinations. Error bars represent standard deviations. (C) Western blot. Cell lysate was examined by Western blotting with anti-human Htt antibody (MAB2166; Chemicon) as in Fig. 3. After detection of signals, the expression of GAPDH as a control was also examined by anti-GAPDH antibody (AM4300; Ambion).

Western blot analyses indicate that a polypeptide of approximately 350 kDa, which is almost the same as the molecular weight estimated from the amino acid sequence (346 kDa) in the *Cj-Htt* cDNA, can be detected in the common marmoset specimens by the antibodies tested, suggesting that the Cj-Htt protein is detectable with the antibodies (Figs. 3A–C). The 350 kDa mouse Htt protein was detected by the MAB2166 antibody (Fig. 3A), but hardly with the other antibodies (Figs. 3B and C). This may be caused by possibly low expression level of mouse Htt in the brain tissue, and/or by difference in the epitope sequences between the common marmoset and mouse Htt proteins. Other than the 350 kDa band, a few bands migrated faster than the 350 kDa band were also observed. They may be degradation products of the Htt protein, and different cells and/or species might have different degradation of the protein. To clarify these, further studies need to be carried out.

In addition to the Htt protein, we also examined the expression of amyloid precursor protein (App) with the 22C11 antibody, which can recognize the same amino acid sequence at positions 66–81 of either the human or mouse App. As a result, the App signal was able to be detected in either the common marmoset or mouse brain tissue, but not in the common marmoset immortalized peripheral blood mononuclear cells (PBMCs) (Fig. 3D), suggesting little or no expression of App in PBMCs and availability of the antibody for detection of the Cj-App protein.

3.3. Gene silencing against the Cj-Htt gene

To verify the data presented here and tools for the detection of *Cj-Htt*, we carried out gene silencing against the expression of endogenous *Cj-Htt* by means of RNA interference (RNAi), and assessed the knockdown potency of designed siRNA targeting *Cj-Htt* using the tools evaluated above. Based on a previous study where a competent siRNA duplex, siRNA-HDexon 1, conferring strong inhibition against the expression of the human *Htt* gene was used (Liu et al., 2003), we chemically synthesized an siRNA duplex, cjHtt-1 siRNA, corresponding to the siRNA-HDexon 1 duplex; note that there is one nucleotide change between cjHtt-1 siRNA and siRNA-HDexon 1 (Fig. 4A).

To examine the effect of the siRNA duplex on gene silencing, we constructed a reporter plasmid carrying the 5′ terminal region of *Cj-Htt* cDNA linked with the *GFP* reporter gene (the 5′*Cj-Htt-GFP* fusion gene). The reporter plasmid and the siRNA were cotransfected into mouse Neuro2a cells, and the expression of the 5′*Cj-Htt-GFP* fusion gene was examined by a fluorescent microscope. As shown in Fig. 4B, the data indicated that the cjHtt-1 siRNA duplex was able to induce strong RNAi activity against the fusion gene expression.

Next, we introduced the cjHtt-1 siRNA duplex into immortalized common marmoset mononuclear cells by means of electroporation, and two days after transfection, the expression levels of the endogenous *Cj-Htt* mRNA and protein were examined by RT-real time PCR and Western blotting, respectively. As shown in Fig. 5, the results consistently indicated that *Cj-Htt* mRNA (A and B) and protein (C) levels markedly decreased in the presence of the cjHtt-1 siRNA duplex, i.e., potent RNAi knockdown against the endogenous *Cj-Htt* gene was induced by the siRNA duplex. Finally, the data presented here also indicate that proper detection of the newly identified *Cj-Htt* gene and its products can be performed by means of the methods and tools assessed in this study.

In conclusion, we described for the first time the common marmoset *Htt* gene, and also detection methods and tools for the gene and its gene products. The data presented here may assist us in promoting a non-human primate HD model with the common marmoset.

Acknowledgments

We would like to thank Dr. R.C. Desrosiers for kindly providing HS viruses. We also thank Drs. K. Nakamura, T. Kabuta, M. Suzuki, and C. Konya for their helpful advice and discussion. Finally, we would like to thank Dr I. Kanazawa for his encouragement and helpful advice. This work was supported by research grants from the Ministry of Health, Labour and Welfare of Japan.

References

Akari, H., et al., 1996. In vitro immortalization of Old World monkey T lymphocytes with Herpesvirus saimiri: its susceptibility to infection with simian immunodeficiency viruses. Virology 218, 382–388.

Andrade, M.A., Bork, P., 1995. HEAT repeats in the Huntington's disease protein. Nat. Genet. 11, 115–116.

Deisboeck, T.S., et al., 2003. Development of a novel non-human primate model for preclinical gene vector safety studies. Determining the effects of intracerebral HSV-1 inoculation in the common marmoset: a comparative study. Gene Ther. 10, 1225–1233.
Doods, H., et al., 2000. Pharmacological profile of BIBN4096BS, the first selective small molecule CGRP antagonist. Br. J. Pharmacol. 129, 420–423.
Gilliam, T.C., et al., 1987. A DNA segment encoding two genes very tightly linked to Huntington's disease. Science 238, 950–952.
Gusella, J.F., et al., 1983. A polymorphic DNA marker genetically linked to Huntington's disease. Nature 306, 234–238.
Huntington's-Disease, C.R.G.o., The Huntington's Disease Collaborative Research Group, 1993. A novel gene containing a trinucleotide repeat that is expanded and unstable on Huntington's disease chromosomes. Cell 72, 971–983.
Kazemi-Esfarjani, P., Benzer, S., 2000. Genetic suppression of polyglutamine toxicity in Drosophila. Science 287, 1837–1840.
Kendall, A.L., Rayment, F.D., Torres, E.M., Baker, H.F., Ridley, R.M., Dunnett, S.B., 1998. Functional integration of striatal allografts in a primate model of Huntington's disease. Nat. Med. 4, 727–729.
Liu, W., Goto, J., Wang, Y., Murata, M., Wada, K., Kanazawa, I., 2003. Specific inhibition of Huntington's disease gene expression by siRNAs in cultured cells. Proc. Jpn. Acad. 79, 293–298.
Lunkes, A., Mandel, J.L., 1998. A cellular model that recapitulates major pathogenic steps of Huntington's disease. Hum. Mol. Genet. 7, 1355–1361.
Mangiarini, L., et al., 1996. Exon 1 of the HD gene with an expanded CAG repeat is sufficient to cause a progressive neurological phenotype in transgenic mice. Cell 87, 493–506.
Neuwald, A.F., Hirano, T., 2000. HEAT repeats associated with condensins, cohesins, and other complexes involved in chromosome-related functions. Genome Res. 10, 1445–1452.
Palfi, S., et al., 2007. Expression of mutated huntingtin fragment in the putamen is sufficient to produce abnormal movement in non-human primates. Mol. Ther. 15, 1444–1451.
Sakai, T., Hohjoh, H., 2006. Gene silencing analyses against amyloid precursor protein (APP) gene family by RNA interference. Cell Biol. Int. 30, 952–956.
t'Hart, B.A., Vervoordeldonk, M., Heeney, J.L., Tak, P.P., 2003. Gene therapy in nonhuman primate models of human autoimmune disease. Gene Ther. 10, 890–901.
von Horsten, S., et al., 2003. Transgenic rat model of Huntington's disease. Hum. Mol. Genet. 12, 617–624.
Walker, F.O., 2007. Huntington's disease. Lancet 369, 218–228.
Yang, S.H., et al., 2008. Towards a transgenic model of Huntington's disease in a non-human primate. Nature 453, 921–924.

Mol Biol Rep
DOI 10.1007/s11033-008-9330-4

Variation of gene silencing involving endogenous microRNA in mammalian cells

Yoshiko Tamura · Mariko Yoshida · Yusuke Ohnishi · Hirohiko Hohjoh

Received: 22 May 2008 / Accepted: 30 July 2008

Abstract MicroRNAs (miRNAs) are small noncoding RNA and play a role in gene expression regulation by inhibiting translation of their target messenger RNAs (mRNAs). In this study, we investigated the effects of endogenous *let-7* miRNA on the expression of target genes in various mammalian cells by means of two types of reporter plasmids possessing target sequences for *let-7*: one carries perfectly matched target sequence for *let-7* in the 3′-untranslated region of the *luciferase* reporter gene to monitor RNA interference (RNAi) activity and the other has three bulged binding sites for *let-7* to monitor translation-inhibition activity. The results indicate that different cells have different levels of gene silencing against the target reporter genes. The data presented here suggest that not only microRNA level but also target transcript level likely participate in the generation of a variety of gene silencing.

Keywords MicroRNA · *Let-7* · Gene silencing · Variation · Target gene expression

Y. Tamura · M. Yoshida · Y. Ohnishi · H. Hohjoh (✉)
National Institute of Neuroscience, NCNP, 4-1-1 Ogawahigashi, Kodaira, Tokyo 187-8502, Japan
e-mail: hohjohh@ncnp.go.jp

Y. Ohnishi
Department of Human Genetics, Graduate School of Medicine, The University of Tokyo, 7-3-1 Hongo, Bunkyo-ku, Tokyo 113-0033, Japan

Introduction

MicroRNAs (miRNAs) are small noncoding RNA, with a typical length of 19–23 nt, which are processed from longer transcripts by digestion with a microprocessor complex containing Drosha and Pasha in the nucleus and Dicer in the cytoplasm [1–3]. Hundreds of miRNA genes have been found in various species [3–5], and their tissue- or organ-specific expression has been detected [5–7]. After Dicer processing, miRNA duplexes undergo strand selection and then the single-stranded mature miRNA elements are incorporated into the RNA-induced silencing complex (RISC) and function as mediators in suppression of gene expression [8–10]. There are two types of gene silencing involving endogenous miRNAs: one is the inhibition of translation of target mRNAs carrying partially complementary fragments to miRNAs in their 3′ untranslated regions (3′UTRs) [11–15], and the other is the digestion of target RNAs which are perfectly or nearly complementary to miRNAs, such as RNA interference (RNAi) [8, 11, 16]. The gene silencing involving miRNAs play an important role in regulation of gene expression in development, differentiation and proliferation [4, 7, 17–22]. Recent studies have further suggested significant association of miRNAs with various cancers [23–26].

While many findings and data on miRNAs themselves are accumulating, little is known about their target gene expression. It is of interest and importance to realize the entity of regulation of gene expression involving gene silencing mediated by endogenous miRNAs. In this report, we investigated the effects of endogenous *let-7* miRNA on the expression of target genes in various mammalian cells by using reporter plasmids carrying target sequences for *let-7*. The data indicated that different cells had different levels of gene silencing involving endogenous *let-7*.

Materials and methods

Cell culture

Neuro2a (N2a), PC12D, and HeLa cells were grown as previously described [27, 28]. HEK293 cells were grown in Dulbecco's Modified Eagle's Medium (DMEM) (Wako) supplemented with 10% fetal bovine serum (FBS) (Sigma), 100 U/ml penicillin and 100 μg/ml streptomycin (Sigma). F9 cells were grown in DMEM supplemented with 15% FBS and the antibiotics as described above. SH-SY5Y cells were grown in EMEM/F-12 (1:1 mixture) containing 10% FBS and the antibiotics. All the cells were cultured at 37°C in 5% CO_2-humidified chamber. HEK293 (Registry No. JCRB9068) and F9 (Registry No. JCRB0001) cells were purchased from the Health Science Research Resources Bank. SH-SY5Y (Registry No. CRL-2266) cells were purchased from the American Type Culture Collection.

Construction of reporter plasmids

To examine the effects of endogenous *let-7* on gene silencing against its target genes, we constructed reporter plasmids with the psiCHECK-2 plasmid (Promega) carrying the *Renilla* and *Photinus luciferase* genes. The plasmid was digested with *Xho* I and *Pme* I, and subjected to ligation with synthetic oligonucleotide duplexes carrying target sequences for *let-7* (the sequences of the oligonucleotides are indicated below). The resultant plasmids carry perfectly matched target sequence (PMTS) and three bulged binding sites (3xBBS) for *let-7* (Fig. 1). We further constructed reporter plasmids by replacing the Bgl II–Nhe I region containing the simian virus 40 (SV40) promoter in the above plasmids with the Bgl II–Nhe I fragment encoding the herpes simplex virus thymidine kinase (TK) promoter isolated from the phRL-TK plasmid (Promega); the resultant reporter plasmids carry the TK promoter linked with the *Renilla luciferase* gene (Fig. 1).

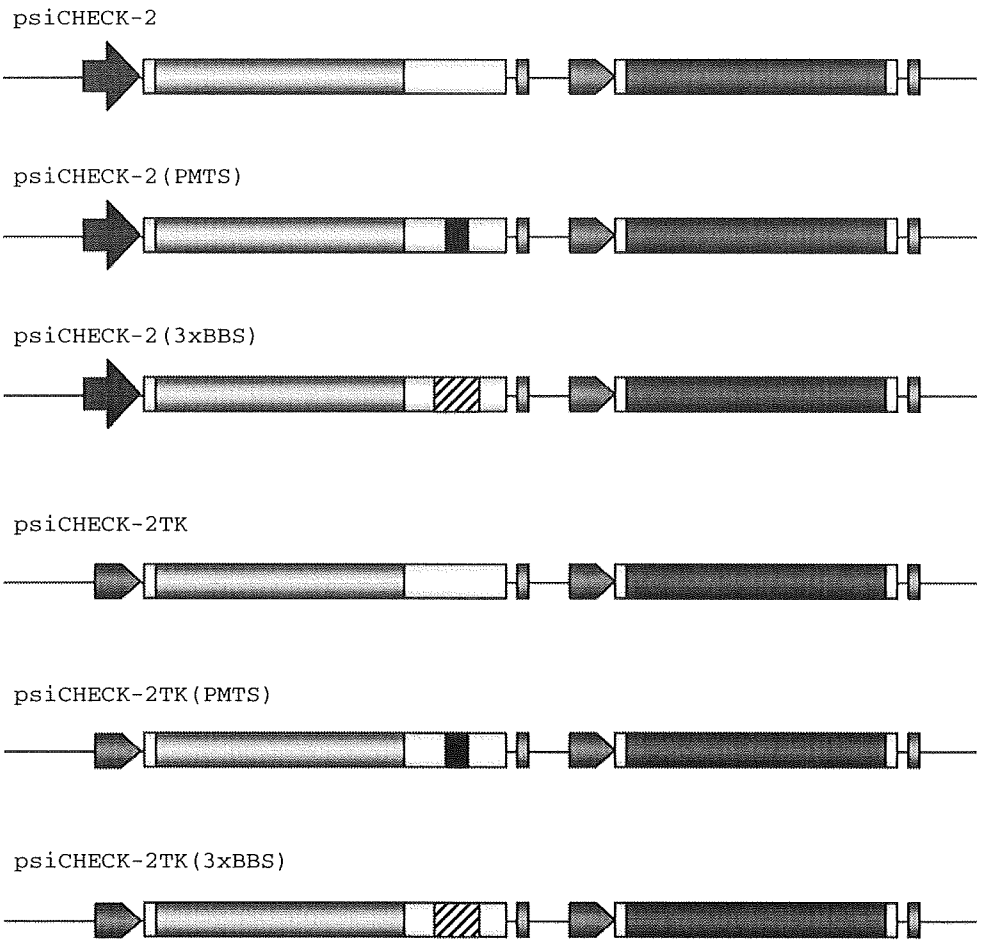

Fig. 1 Constructs of reporter plasmids. Reporter plasmids were constructed based on the psiCHECK-2 plasmid (Promega). Yellow, green, gray and pink boxes indicate the *Renilla* and *Photinus luciferase* coding regions, untranslated region, and poly(A) signal, respectively. Red arrow and orange pentagon indicate the SV40 and TK promoters, respectively. Solid and hatched boxes represent perfectly matched target sequence (PMTS) and three bulged binding sites (3 × BBS) for *let-7*, respectively

The sequences of the oligonucleotides synthesized are as follows:

Ss-let-7(PMTS): 5′-TCGAGAACTATACAACCTACT ACCTCATTACTAGT-3′
As-let-7(PMTS): 5′-ACTAGTAATGAGGTAGTAGGT TGTATAGTTC-3′
Ss-let-7(3 × BBS): 5′-TCGAGGGACAGCCTATTGA ACTACCTCACTCGGAGCACAGCCTATTGAACTAC CTCAGGCCTGCACAGCCTATTGAACTACCTCATT ACTAGT-3′
As-let-7(3 × BBS): 5′-ACTAGTAATGAGGTAGTTC AATAGGCTGTGCAGGCCTGAGGTAGTTCAATAG GCTGTGCTCCGAGTGAGGTAGTTCAATAGGCTGT CCC-3′

Transfection and reporter assay

Transfection of the reporter plasmids was carried out using Lipofectamine 2000 transfection reagent (Invitrogen) according to the manufacturer's instructions, and to each well (24-well culture plates) 0.1 μg of each reporter plasmid was applied. Forty-eight hours after transfection, cell lysate was prepared and the expression levels of luciferases were examined by the Dual-Luciferase reporter assay system (Promega), according to the manufacturer's instructions. The reporter plasmids were also transfected together with either Pre-miR miRNA precursor (Production ID: PM10048; Ambion) or Anti-miR miRNA inhibitor (Production ID: AM10048; Ambion) of *let-7a* into cells, and then the expression of the reporter genes were examined as described above.

Reverse transcription-(real time) polymerase chain reaction (RT-(real time) PCR)

Total RNA was extracted from cells with Trizol reagent (Invitrogen) and subjected to RT-(real time) PCR. Real-time PCR was carried out by means of the AB 7300 Real Time PCR System (Applied Biosystems) with a TaqMan Universal PCR Master Mix together with Assays-on-Demand Gene Expression products (Applied Biosystems) or a SYBR Green PCR Master Mix together with Perfect Real Time Primers (TAKARA BIO), according to the manufacturers' instructions. The Assays-on-Demand Gene Expression products and Perfect Real Time Primers used are shown in Tables 1 and 2, respectively.

To examine the expression levels of *let-7a* and *5sRNA* as a control, total RNA was subjected to RT-PCR using the mirVana qRT-PCR detection kit (Ambion). Real-time PCR was performed by the AB 7300 Real Time PCR system (Applied Biosystems) with SuperTaq polymerase (Ambion). End-point PCR analysis after RT reaction was also carried out by the GeneAmp PCR system 9700 (Applied Biosystems) according to the manufacturer's instructions. The resultant PCR products were electrophoretically separated on 12% polyacrylamide gels and visualized by ethidium bromide staining.

Table 1 Assays-on-demand gene expression products used in this study

Human genes		Mouse genes	
Gene name	Assay ID	Gene name	Assay ID
EIF2C1	Hs00201864_m1	*Eif2c1*	Mm00462977_m1
EIF2C2	Hs00293044_m1	*Eif2c2*	Mm00838341_m1
EIF2C3	Hs00227461_m1	*Eif2c3*	Mm00462959_m1
EIF2C4	Hs00214142_m1	*Eif2c4*	Mm00462659_m1
DICER	Hs00229023_m1	*Zfp36*	Mm00457144_m1
ZFP36	Hs00185658_m1	*Trc6a*	Mm00523487_m1
TRC6A	Hs00379422_m1	*Gapdh*	Mm99999915_g1
GAPDH	Hs99999905_m1		

Table 2 Perfect real time primers used in this study

Human genes		Mouse genes	
Gene name	Primer-Set ID	Gene name	Primer-Set ID
TARBP2	HA039221	*Dicer*	MA043537
PRKRA	HA038462	*Tarbp2*	MA027351
		Prkra	MA030829

DNA chip analysis

Total RNA was extracted from cultured cells using Trizol reagent (Invitrogen). For preparation of cellular miRNAs, small-sized RNAs containing miRNAs were isolated from total RNA using the RNeasy MinElute Cleanup kit (Qiagen). The isolated small-sized RNAs (~1 μg) were subjected to direct labeling with a fluorescent dye using the Platinum*Bright* 647 Infrared nucleic acid labeling kit (KREATECH), according to the manufacturer's instructions. After labeling, the labeled RNAs were purified from free fluorescent substrates by KREA*pure* columns (KREATECH) and used in hybridization. Hybridization was carried out with the *Genopal*®-MICM DNA chips (Mitsubishi Rayon) for detection of mouse miRNAs as described previously [27, 29]. After hybridization, the DNA chips were washed twice in 2 × SSC containing 0.2% SDS at 50°C for 20 min followed by washing in 2 × SSC at 50°C for 10 min, and then hybridization signals were examined and analyzed by means of a DNA chip reader adopting multi-beam excitation technology according to the manufacturer's instructions (Yokogawa Electric Corporation).

Results and discussion

Different cells have different levels of gene silencing mediated by endogenous *let-7*

In order to examine the effects of endogenous miRNAs on the expression of their target genes, we chose the *let-7* miRNA since it had been studied well and because it appeared to be expressed ubiquitously. To investigate the effects of endogenous *let-7* on the expression of its target genes, we performed widely-used assay with luciferase reporter genes carrying target sequences for miRNAs, by which gene silencing with mRNA digestion and translation inhibition mediated by miRNAs can be detected [11, 14, 15, 21, 30–34]. In this study, two types of reporter plasmids were constructed: one carries perfectly matched target sequence (PMTS) for *let-7* in the 3′UTR of the *Renilla luciferase* reporter gene to monitor RNAi activity and the other has three bulged binding sites (3 × BBS) for *let-7* to monitor translation-inhibition activity (Fig. 1), according to the previous studies described by Pillai et al. [14] and Schmitter et al. [34], where the target sequences were shown to undergo distinct gene silencing to each other as described above. The reporter plasmids and empty vector (psiCHECK-2 or psiCHECK-2TK) as a control were transfected into various mammalian cells, and expression of the reporter genes was examined. Figure 2 shows the results. When the target reporter gene carrying PMTS was examined, the expression of the reporter gene (carrying PMTS) was strongly inhibited in the cells except F9 cell, suggesting that potent RNAi activity mediated by endogenous *let-7* occurred in the cells. Interestingly, when the

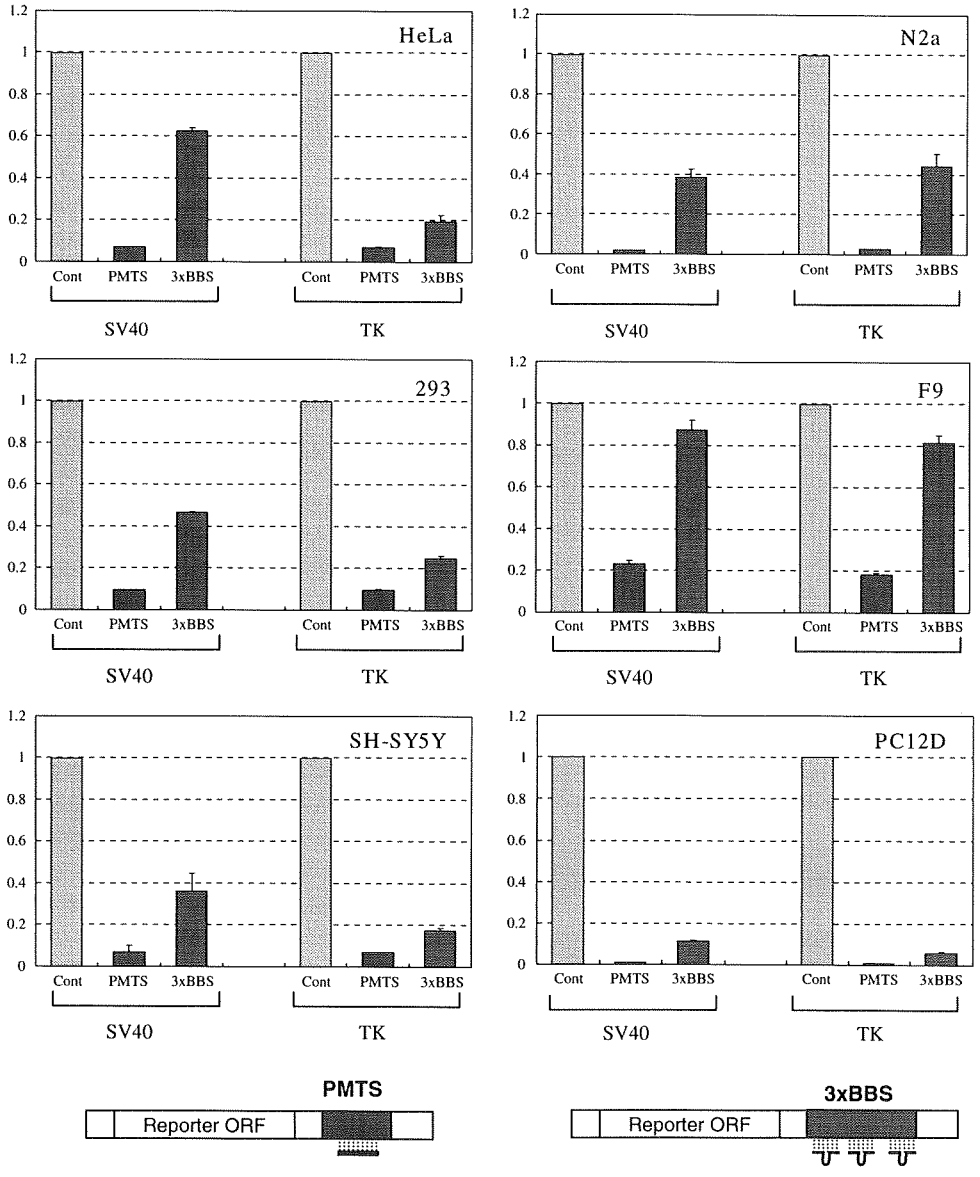

Fig. 2 Knockdown potency of gene silencing mediated by endogenous *let-7*. Reporter genes carrying perfectly matched target sequence (PMTS) and three bulged binding sites (3 × BBS) for *let-7* were constructed (Fig. 1), which are schematically shown together with *let-7* represented by a solid bar or crooked lines. The reporter genes were introduced into indicated cells, and the expression levels of the reporters were examined. Ratios of normalized target (*Renilla*) luciferase activity to control (*Photinus*) luciferase activity are shown: the ratios of luciferase activity in the presence of either PMTS (green bars) or 3 × BBS (pink bars) are normalized to the ratio obtained with the psiCHECK-2 or psiCHECK-2-TK empty plasmid (gray bars) as a control. Data are averages of at least four independent experiments. Error bars represent standard deviations. The SV40 and TK promoters, which drive the reporter genes (Fig. 1), are indicated

reporter gene carrying 3 × BBS was investigated, the level of expression of the target reporter gene varied among the cells, i.e., different cells had different levels of suppression against the target gene. Of the cells investigated, F9 cell exhibited the weakest suppression of the target reporter genes for *let-7*.

Various expression levels of endogenous *let-7* among the cells

In order to address why different cells had different levels of gene silencing (Fig. 2), we investigated the expression of endogenous *let-7* in the cells by means of RT-PCR using specific primers for *let-7a*. As shown in Fig. 3, the results of end-point PCR analyses revealed that the level of *let-7a* varied among the cells: PC12D and SH-SY5Y cells appear to express *let-7a* in a higher level and F9 cell may hardly express it. F9 cell together with N2a cell as a control were further examined by RT-real time PCR followed by analysis with the cycle threshold (Ct) method, and the results suggested that F9 cell might express approximately one-sixth to one-eighth as much *let-7a* as N2a cell (data not shown). We also examined expression profiles of the *let-7* family members by means of the *Genopal*-MICM DNA chips, where DNA probes for the *let-7* members (the mouse *let-7a-g* and *-7i*) are installed. The results of the expression profile analysis indicated that not only *let-7a* but also other *let-7* members were barely present in F9 cell (Fig. 4).

Based on the results, it should be noted that there is a possible correlation between the expression level of *let-7* (Figs. 3, 4) and the suppression level of the target reporter genes (Fig. 2). Data consistent with the possibility were also obtained from experiments with an anti-*let-7* inhibitor: the expression level of the target reporter gene carrying either PMTS or 3 × BBS was increased with an increasing amount of the anti-*let-7* inhibitor, suggesting the reduction of gene silencing mediated by *let-7* with an increasing amount of the anti-*let-7* inhibitor (Fig. 7a). To further

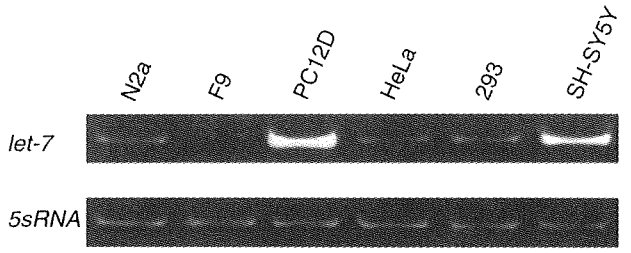

Fig. 3 Expression of endogenous *let-7* in various cells. Total RNA extracted from the indicated cells was subjected to cDNA synthesis, and end-point PCR analysis of *let-7* and *5sRNA* as a control was carried out. The resultant PCR products were examined by electrophoresis with 12% polyacrylamide gels followed by ethidium bromide staining

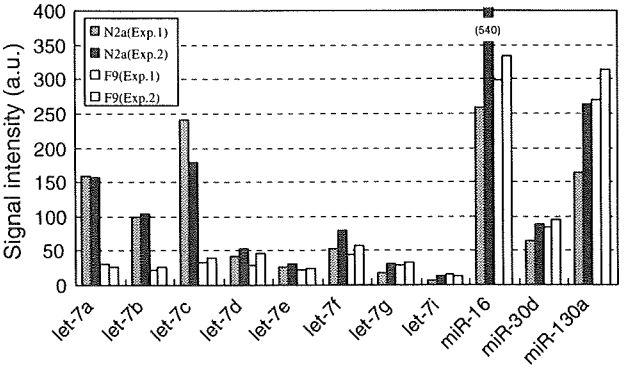

Fig. 4 Expression profiles of *let-7* miRNAs. Small-sized RNAs extracted from F9 and N2a cells were examined by the *Genopal*®-MICM DNA chips (Mitsubishi Rayon). Expression profiles of *let-7* members (indicated) and miR-16, −30d and −130a as positive controls are shown. Hybridization signal intensity of each miRNA was subjected to background subtraction and indicated by arbitrary intensity units (a.u.). The intensity which is over the plotted area is indicated in a parenthesis. Expression profile analysis was repeated individually (Exps. 1 and 2)

evaluate the possibility, we examined the expression of genes associated with RNAi and/or miRNA pathways. The *Ago1-4*, *Dicer*, *Pact*, *Tarbp2*, *Zfp36*, and *Trc6a* genes were investigated by RT-real time PCR (Fig. 5), and the results indicated that the expression profiles of the genes were similar among the cells, suggesting little correlation of the expression of the genes with various suppression levels of the target reporter genes.

Since F9 cell exhibited weak suppression against the target reporter genes for *let-7* (Fig. 2), we examined whether the cell possessed immature gene silencing machinery

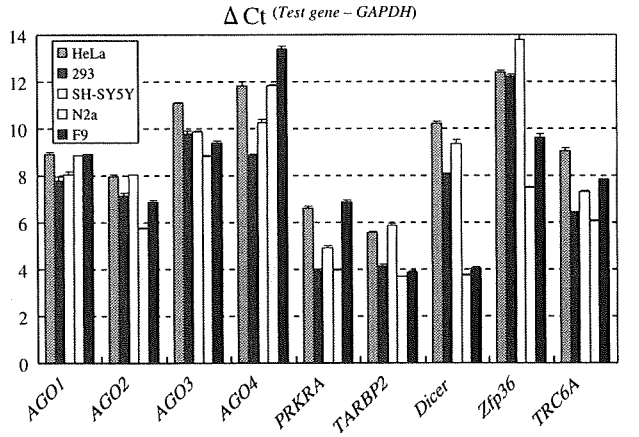

Fig. 5 Expression profiles of genes involved in gene silencing pathways. Total RNA was extracted from indicated cells and examined by RT-real time PCR. The genes examined are indicated. Expression levels of the genes were analyzed by the cycle threshold (Ct) method: the difference between their Ct and the Ct of the *Gapdh* gene examined as a control [$\Delta Ct^{(Test\ gene\ -\ Gapdh)}$] was calculated and plotted. Data are averages of three measurements by RT-real time PCR analyses. Error bars represent standard deviations